Title
ELASTIC SCATTERING OF PI MESONS ON PROTONS IN THE ENERGY REGION 550 TO 1020 Mev

Author
Wood, Calvin D.

Publication Date
1961-10-01

UNIVERSITY OF CALIFORNIA

Ernest O. Lawrence

Radiation Laboratory

BERKELEY, CALIFORNIA

DISCLAIMER

UCRL-9507
UC-34 Physics
TID-4500 (16th Ed.)

cy 2

UNIVERSITY OF CALIFORNIA
Lawrence Radiation Laboratory
Berkeley, California

Contract No. W-74-5-eng-48

ELASTIC SCATTERING OF PI MESONS ON PROTONS IN THE ENERGY REGION 550 TO 1020 Mev

Calvin D. Wood

(Ph. D. Thesis)

October 1, 1961

Printed in USA. Price $2.00. Available from the
Office of Technical Services
U. S. Department of Commerce
Washington 25, D.C.

ELASTIC SCATTERING OF PI MESONS ON PROTONS IN THE ENERGY REGION 550 TO 1020 Mev

Contents

Contents

ELASTIC SCATTERING OF PI MESONS ON PROTONS IN THE ENERGY REGION 550 TO 1020 Mev

Calvin D. Wood

Lawrence Radiation Laboratory
University of California
Berkeley, California

October 1, 1961

ABSTRACT

This experiment measured the differential cross section for elastic scattering of negative π mesons from protons at incident pion kinetic energies of 550, 600, 720, 900, and 1020 Mev. Pions were produced when the Bevatron circulating proton beam struck a copper target. Pions of the requisite momentum were brought to a focus at a liquid hydrogen scattering target by a magnetic system for beam optics. Elastic scattering events were selected from a background of inelastic events by demanding coincidences between pairs of scintillation counters that were placed at the proper kinematical angles to count elastically scattered pions and their corresponding recoil protons.

The resulting angular-distribution curves were least-squares fitted with a cosine power series. A study of the coefficients of the power series allows us to make certain inferences about the angular momentum states contributing to the second and third maxima in the total π^--p cross section which occur at 600 and 900 Mev, respectively. The 600-Mev peak appears to be due to a D state, with a total J value of 3/2 rather than 5/2.

The data at 900 Mev cannot be well explained by a single ($F_{5/2}$) state in resonance, but rather there is strong evidence for at least D and F waves in superposition. The forward "diffraction" peaking of the angular distribution indicates that absorptive processes may be predominant.

I. INTRODUCTION

Early measurements of π^--p total cross sections[1] showed the well-known $P_{3/2,3/2}$ resonance at about 200 Mev laboratory kinetic energy,[2,3] and a broad maximum at about 900 Mev. Later measurements resolved the higher maximum into two separate peaks occurring at 600 and 900 Mev, respectively.[4-8] Corresponding peaks also occur in pion photoproduction at energies of about 750 Mev and 1050 Mev.[9-18] The energy difference between the peaks occurring in photoproduction and in scattering experiments arises because an incident gamma ray must supply the rest mass energy of a pion in addition to the energy of the resonant final states.

Although the 200-Mev peak has been clearly shown to be due to a single state in resonance,[2,3] the 600- and 900-Mev peaks have not been established as pure resonant states. Nevertheless, they are usually referred to as "resonances," despite the fact that the forward-diffraction peaking in the angular distribution for elastic scattering clearly suggests a strong contribution from nonresonant states. If we assume that each peak in the total cross section is due to a resonant state added to a nonresonant background, we can assign orbital and angular momentum quantum numbers (ℓ and J, respectively) to these states. The isotopic spin quantum number is readily fixed at $T = 1/2$, since the peaks do not appear in the π^+-p cross section, which is a pure $T = 3/2$ state.

Early in the history of π^--p scattering studies, when the second and third maxima had not yet been resolved, Dyson[19] proposed a model to account for the broad "second maximum" at about 900 Mev. He felt it unlikely that the phenomenon could be due to a single resonant state because that state would have to have a value for the total angular momentum of at least 11/2. The mechanism he proposes so that several $T = 1/2$ states can give a maximum cross section at 900 Mev involves a resonant π-π state at a relative momentum of 250 Mev/c. If this π-π resonance were in a $T = 0$ state, it would contribute nothing to π^+-p scattering. In addition, the excess inelastic π^--p scattering

would come from the interaction of the incoming pion with a loosely bound cloud meson so that both pions escape from the proton.

Although the accumulation of experimental evidence, including the resolution of the broad peak into two sharper maxima at 600 and 900 Mev, has not borne out all the predictions of Dyson's early model, it is interesting to note that the idea that a π-π interaction is responsible for the high-energy phenomena still actively occupies the thinking of many theorists[20] who are trying to explain the mechanisms of π-p scattering.

There is a vast array of strange particles with interesting interactions between them and the nonstrange particles (e.g., resonances are also-seen in π-hyperon[21] and K-nucleon[22] scattering), and it is felt that there are general principles[23] underlying the interactions of the strongly interacting particles which can best be understood by attacking first the problem of understanding the interaction between pions and nucleons,[24] the particles about which the most is already known. Thus, a complete description of pion-nucleon scattering is very desirable from a theoretical point of view.

The description of the $P_{3/2,3/2}$ resonance is quite complete, and was made in terms of phase shifts and partial waves.[25] At the energies of this experiment, however, we must include orbital angular momentum states at least through F waves, which means that at least 28 parameters must be determined to give a complete phenomenological description of $\pi^{\pm}$-p scattering, i.e., two spin orientations for each angular momentum state (except $\ell = 0$), the real and imaginary parts of the phase shifts for each partial wave (see Appendix A), and, in addition, two possibilities for the value of the isotopic spin of each wave. With so many free parameters to determine, it is doubtful that a partial-wave analysis can be very useful in analyzing the data. Indeed, it is possible to fit a given angular distribution curve with various sets of choices for the values of the parameters, because the problem is not uniquely determined by angular distribution data alone. Other kinds of data, such as charge-exchange scattering, or measurement of the

polarization of the recoil proton, are needed before the problem can be regarded as uniquely determined in a mathematical sense. Even then a partial-wave analysis may not prove to be the best approach to complete understanding, because of the large number of parameters involved.

Elastic scattering experiments have been done in the energy region of the higher peaks,[26-40] but most of them have a relatively low statistical accuracy. The experiment described herein provides more accurate angular distributions (2 to 4% statistics) in the energy region of the higher "resonances" than have previously been known. This experiment also gives angular distributions at energies where no similar experiments have been done.

On the basis of pion photoproduction data, including measurement of the polarization of the recoil proton, Peierls suggested that the lower peak was a $D_{3/2}$ state.[41] He also suggested a possibility of $F_{5/2}$ for the higher peak, including π-nucleon interactions in his considerations.[42] The assignment of quantum states on the basis of previous experimental evidence, and the data of this experiment, is discussed in more detail in Sec. V of this thesis.

II. APPARATUS AND PROCEDURE

A. General Description of the Experiment

The elastic scattering of pions by hydrogen was measured by comparing the difference in scattering by a full and an empty liquid hydrogen target. This procedure corrects automatically for spurious scattering from the target walls or other material in the beam.

Pions from a copper target inside the Bevatron were brought to a hydrogen target by a magnetic beam optical system, and elastic scattering events there were detected by a number of scintillation counters placed about the target.

Figure 1 shows the kinetic energies used in this experiment with respect to the total π^--p cross section; they are 550, 600, 720, 900, and 1020 Mev.

Figure 2 is a plan view of the experiment, and Fig. 3 shows the arrangement of the scintillation counters about the hydrogen target. For each pion counter in Fig. 3 there is a corresponding proton counter, placed at the correct kinematical angle to detect the recoil proton in coincidence with the elastically scattered pion.

Inelastic events that could appear as elastic scattering were corrected for by determining the distribution of inelastic events for pairs of counters that did not have an elastic kinematical relationship, and then interpolating to obtain a value for the background due to inelastic events in the region of elastic events. This background was then subtracted from the raw data to yield the correct number of elastic events.

We measured the number of particles in the pion beam with a coincidence arrangement between two scintillation counters: one counter was placed at the aperture of a quadrupole and was made large enough to count all the particles in the beam; the second was placed just before the hydrogen target, and was made small enough to count only those particles that should pass through the liquid hydrogen target vessel without striking the side walls unless scattered out of the beam. In

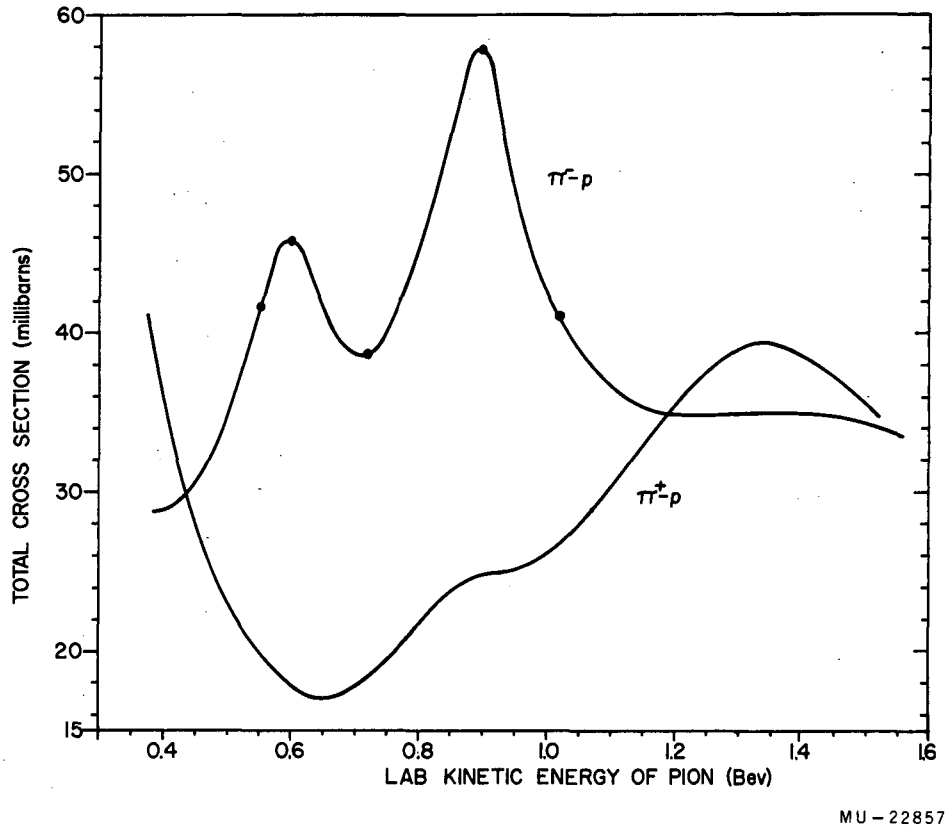

Fig. 1. Total cross sections for $\pi^{\pm}$-p scattering, showing the energies at which angular distributions were measured in this experiment.

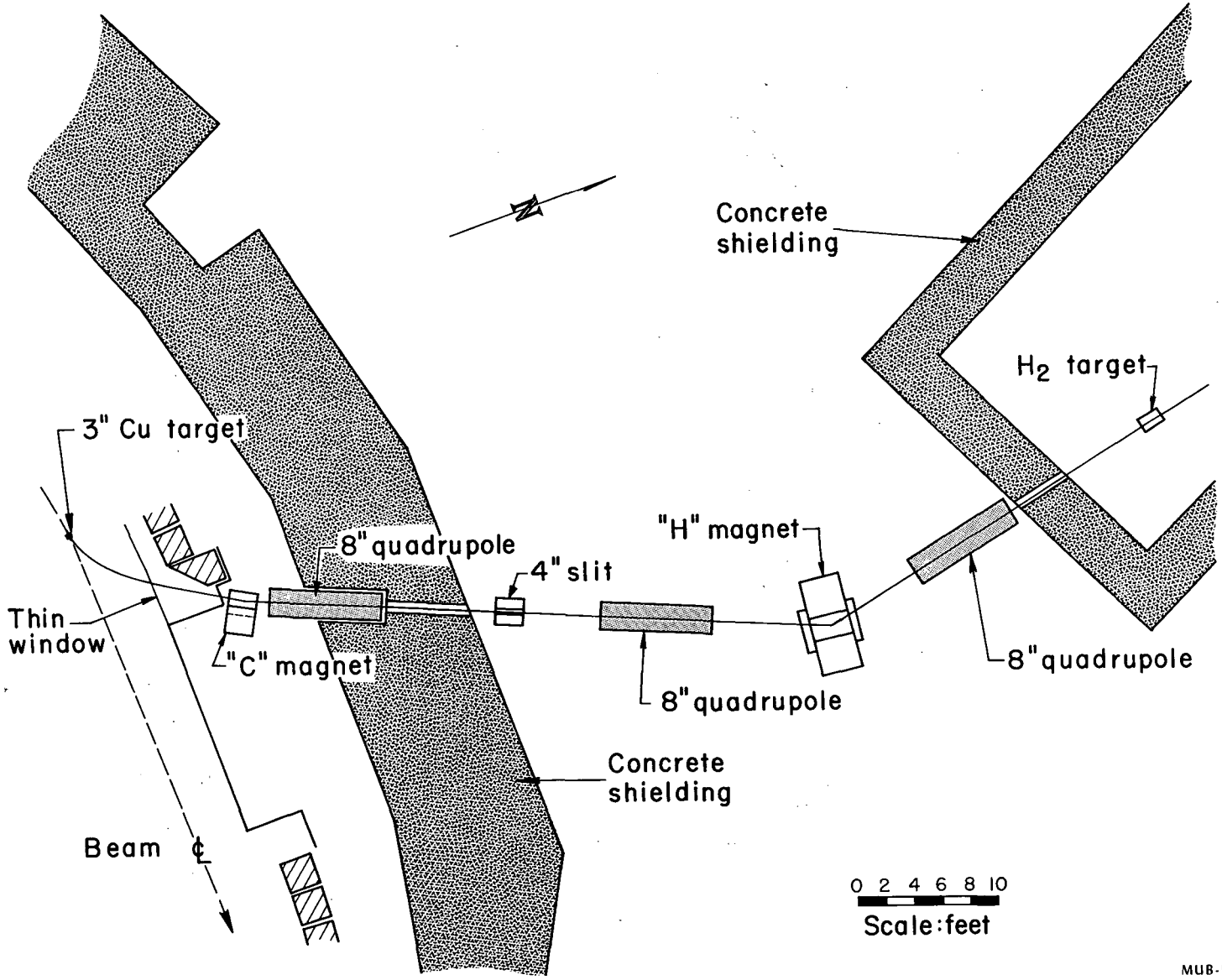

Fig. 2. Plan view of the experimental arrangement, showing the central-ray orbit for a 720-Mev pion. The primary Cu target and the liquid hydrogen target are not drawn to scale.

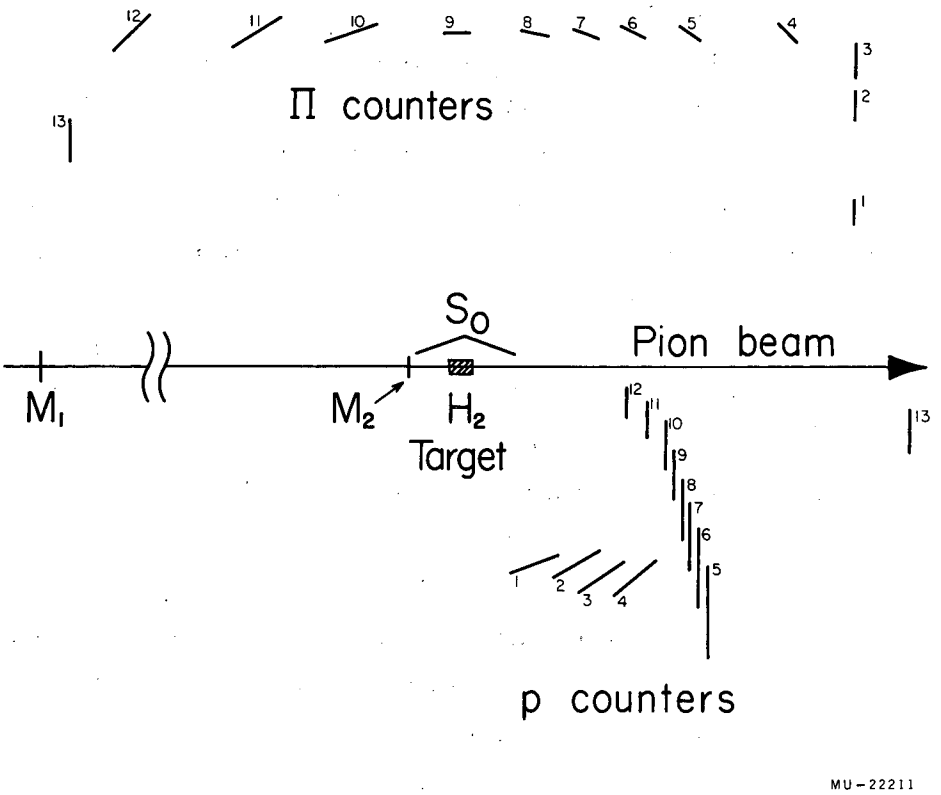

Fig. 3. Arrangement of the scintillation counters about the hydrogen target. The small numbers indicate pairs of counters placed at the correct kinematical angles to detect both particles resulting from an elastic scattering event.

order to correct the beam monitor for spurious counts caused by particles other than pions, we measured the composition of the secondary beam with a gas Cerenkov counter.

B. Experimental Details

1. Pion Source

Pions were produced inside the Bevatron by collisions between the circulating proton beam and a copper "target." In Appendix B we discuss the criteria we considered in choosing a Bevatron target.

The "target" was a collection of three separate targets that could be raised independently from the floor of the vacuum tank. There were three target positions contributing to the five energies of the experiment. Figure 4 shows the central-ray orbits for negatively charged particles of momenta 690, 743, 864, 1045, and 1166 Mev/c. The small take-off angle was chosen to maximize the pion flux at the hydrogen target, as the pions are strongly peaked forward in the laboratory system.

The target had the following dimensions: 3 in. along the beam line; 1/2 in. wide, and tapering from 1/2-in. height at the inner radius to 1/4-in. height at the outer radius. Since the circulating proton beam strikes the target first at its outer radius, we felt that a 1/4-in. target would give us a sharper object in the vertical direction, but at the same time we wanted the larger dimension at the inner radius to be able to use those particles that did not lie in the median plane of the Bevatron.

a. Beam Spill Effects. This experiment was run simultaneously with a bubble chamber experiment. For the greater part of the running we used alternate pulses as well as a part of each bubble chamber pulse. The most desirable beam spill for bubble chamber work is a "spike" in time, so that all the particles entering the chamber do so simultaneously (i.e., particles produced inside the Bevatron should all come from the same point in time). The best beam for a counter experiment, on the other hand, is spread out in the time as much as possible to reduce the

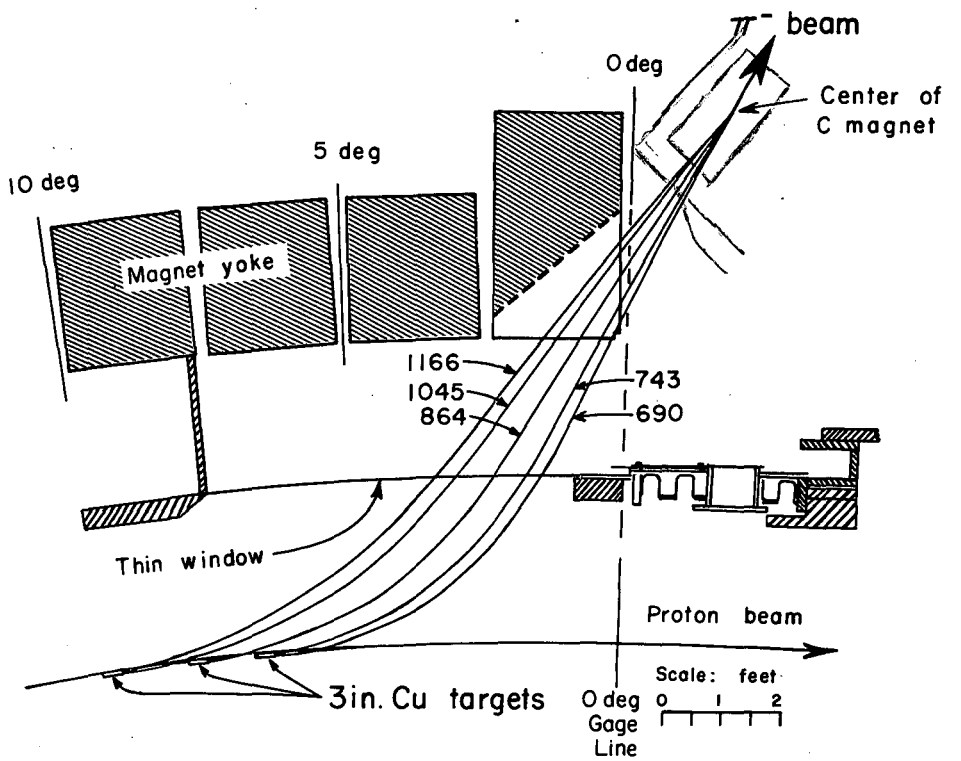

Fig. 4. Central-ray orbits for particles of various momenta, produced in the primary target inside the Bevatron. The numbers associated with the orbits indicate the momentum in the units of Mev/c.

instantaneous counting rate. The two kinds of beam spill are shown in Fig. 5.

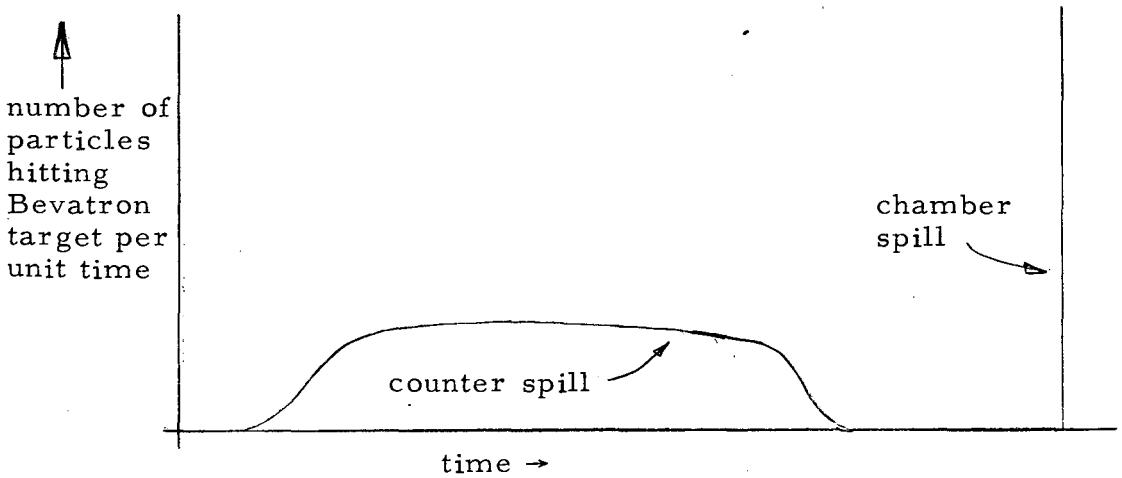

Fig. 5. Beam Spill

The tracking apparatus of the Bevatron apparently could not give both types of spill consistently and still optimize the most desirable aspects of each, because a great deal of rf structure was apparent in the counter spill, from time to time. The amount of this rf structure varied over a wide range of values, as determined from an oscilloscope that was triggered on a signal from the induction electrode and whose input was from a single scintillation counter placed in the pion beam. For further discussion of rf structure, see Sec. III-B-8 (Beam Composition–Normalization) of this thesis.

2. Magnet System and Beam Optics

The magnet system shown in Fig. 6 contained: a 12×24-in. bending magnet C; three 8-in.-bore focusing quadrupole triplets (Q_1, Q_2, Q_3); and an 18×36-in. bending magnet H.

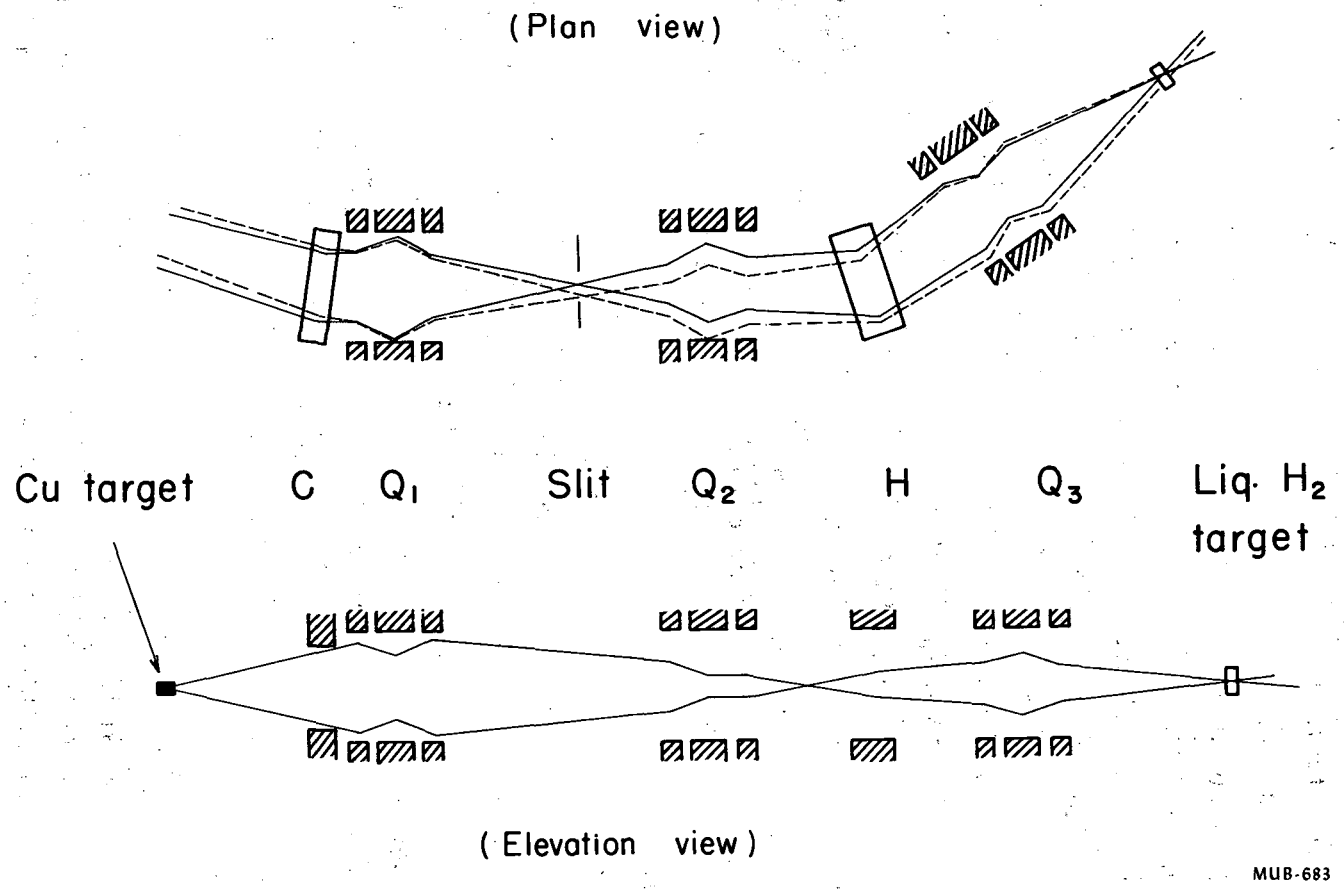

Fig. 6. Magnet beam optical system showing extreme rays of the pion beam. The dotted lines in the plan view are for particles of momentum differing by 1% from the correct momentum. The horizontal scale is greatly compressed with respect to the vertical. The targets are not drawn to scale.

As Fig. 4 shows, beams of different momenta enter C at different angles. The field in C was adjusted to guide particles of the desired momentum down the established beam line.

The effective solid angle from the copper target, as seen by Q_1, was about 1 msr.

Q_1 brought rays of the correct momentum to a horizontal focus between Q_1 and H. Rays of slightly different momenta were deflected a greater or less amount by the Bevatron's main field and by the field in C, and hence were brought to a focus to one side or the other of the main beam line. The momentum spread of the pion beam (±2%) was determined by placing a collimating slit at the position of this focus. The momentum dispersion of the pions at the slit, due to bending in the Bevatron and C, was largely compensated for by the bending in H. In Fig. 6 the solid lines represent the extreme rays for particles of the correct momentum, and the dashed lines represent the extreme rays for particles whose momentum differs from the correct momentum by 1%. As Fig. 6 also shows, there is a momentum focus at the hydrogen target.

Because of the focal properties of the magnetic field of the Bevatron in the horizontal plane, the pion source appeared as a slightly blurred and distorted virtual object near infinity, but there was almost no distortion of the source in the vertical plane. Thus, the image of the pion beam at the liquid hydrogen target was smeared out horizontally, so that the beam intensity fell off by only a factor of two at a horizontal distance of 2 inches from the beam center line, but was down by a factor of two at a distance of only 1 inch vertically from the center line.

Q_2, operated as a field lens between Q_1 and Q_3, increased the flux at the hydrogen target by about a factor of two.

The deflection of the beam through H, the final momentum selector for the system, was measured with the magnet in place by wire orbiting before and after the experiment. These measurements agreed to within ±0.5%. The angle of bend was 35 deg. The horizontal focusing effect of bending magnets was eliminated by orienting H so

that the beam center line made equal entrance and exit angles with respect to the field. Vertical focusing effects were compensated for by the action of Q_3, since the vertical and horizontal focal lengths of a quadrupole can be varied independently.

The currents in the quadrupoles were determined before the experiment by means of an IBM 650 computer program.[43] During the experiment, the magnet system was tuned up to maximize the flux of particles incident on the hydrogen target. The magnet current values determined by the tune-up were within 2% of the calculated values.

Figure 7 is a photograph of Q_2, H, and Q_3, and in the background shows the concrete shielding house that was built around the hydrogen target.

3. Hydrogen Target

With the exception of the target vessel, the hydrogen target used in this experiment was the same as the one described in Ref. 44.

The target vessel was a 0.0075-in.-thick Mylar right cylinder 4 in. long and 2 in. in diameter. A stainless steel ring about the vessel contained the fittings for the fill and empty tubes. Eight layers of 0.00025-in. aluminized-Mylar heat shielding were wrapped around the vessel and placed inside the vacuum chamber wall. Small holes were cut in the heat shielding to allow visual positioning of the target. The amount of Mylar in g/cm^2 traversed by the beam was about one-eighth the amount of liquid hydrogen traversed by the beam when the vessel was filled.

The vacuum chamber was designed so that there were no obstructions around the vessel within an angular range of 270 deg in θ and 18 deg in ϕ (see Sec. II-4, Scintillation Counters, for a definition of these angles). The wall of the chamber consisted of two layers of 0.010-in. Mylar.

Figure 8 shows a plan view and Fig. 9 an elevation view of the hydrogen target vessel and surrounding vacuum chamber. The vessel was emptied by closing a valve on the tube marked "To boiloff" in Fig. 9. Then, as the liquid hydrogen in the flask boiled, the expanding gas forced the liquid down into the tube leading to the reservoir.

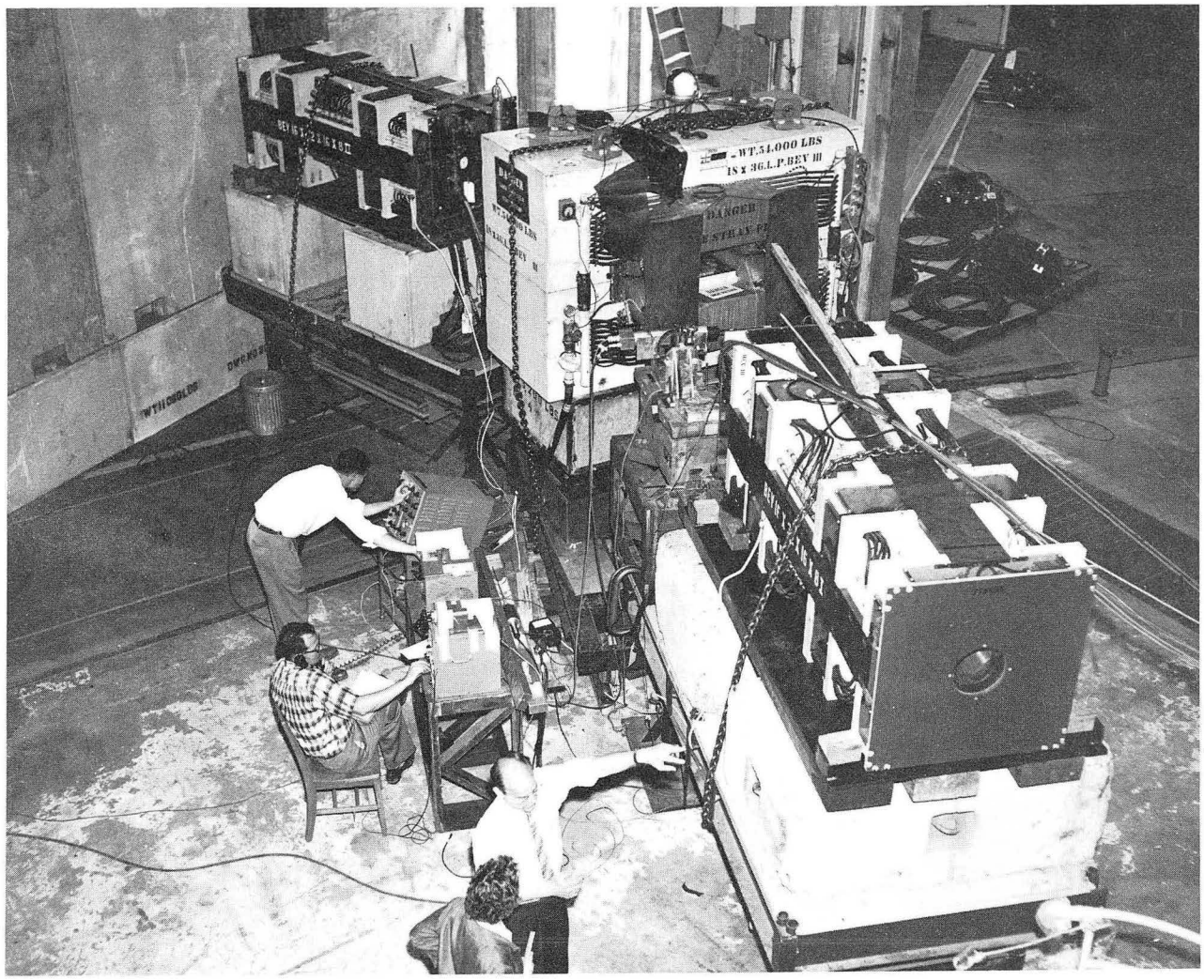

ZN-2946

Fig. 7. Picture of magnets Q_2, H, and Q_3, taken while field measurements were being made in Q_3.

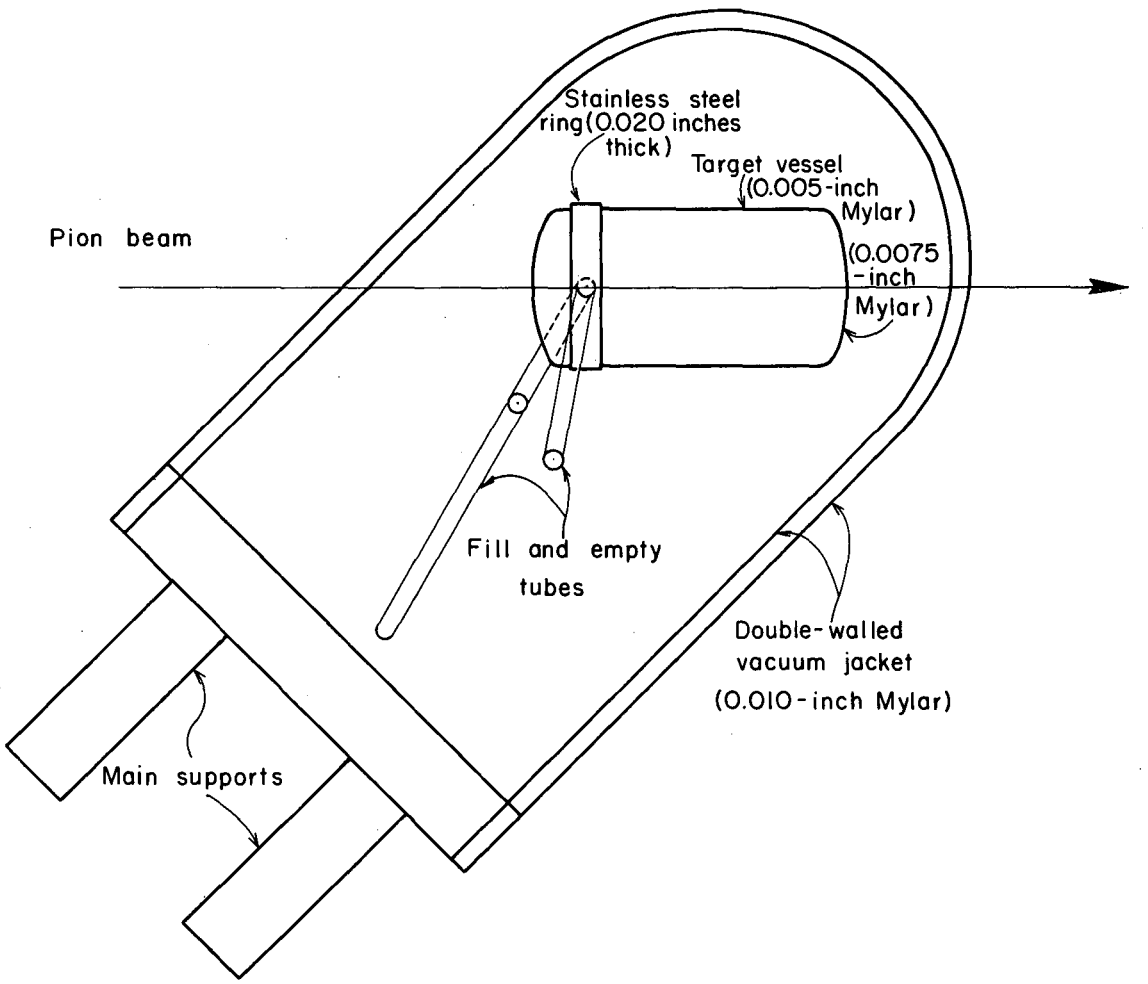

Fig. 8. Plan view of the liquid hydrogen target vessel. All plumbing and supports are positioned to provide a 270-deg unobstructed region for the detection of the scattered particles.

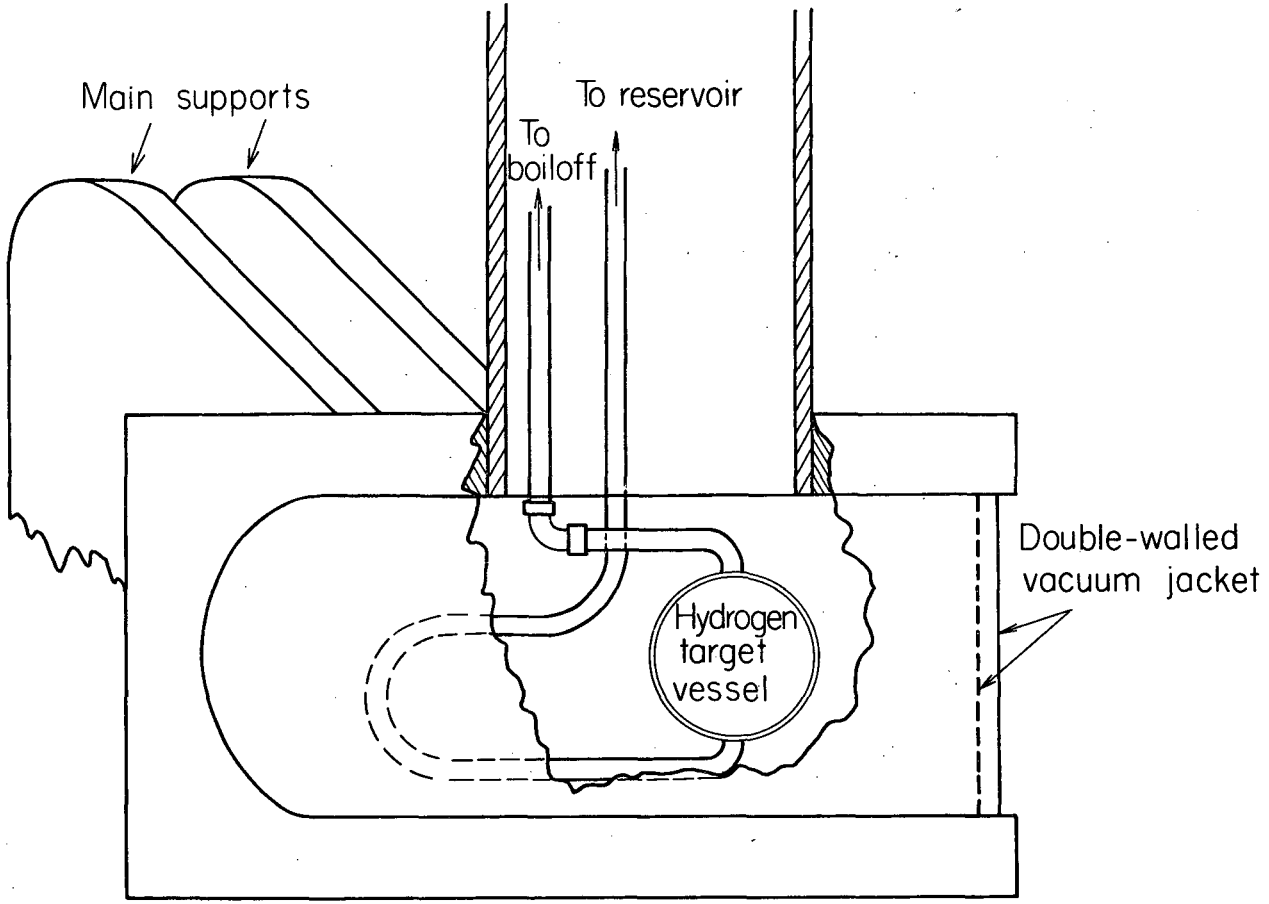

Fig. 9. Elevation view of the hydrogen target vessel looking upstream along the beam line.

The target was filled by opening the same valve, which was solenoid-operated so that the target could be filled and emptied by remote control from the counting area, as a safety precaution.

The target vessel was measured with micrometer calipers while it was full of N_2 at a positive pressure of 1 atmos. The measurement, repeated several times, had an error of one part in 4000.

4. Scintillation Counters

The scintillation counters were made of a solid solution of terphenyl in polystyrene, and were shaped to approximate sections on the surface of a sphere centered at the hydrogen target. Photomultiplier tubes (RCA 6810A) were used to view the scintillators through lucite light pipes. Extra-high-capacitance tube bases were used on all counters that were exposed to the main pion beam, because of the high singles counting rate. High-capacitance bases were used on all the other scintillation counters.

We used the following spherical coordinate system to describe the position of the scintillation counters with respect to the hydrogen target, whose center was the origin: R was the radius vector to the center of a counter; θ was the angle between R and the polar axis, which coincided with the central ray of the pion beam; ϕ was the azimuthal angle between the direction of the scattered pion and the horizontal plane which contained the polar axis; θ_3 and θ_4 were the angles of scatter of the pion and proton, respectively, in the laboratory system (see Fig. 10, below).

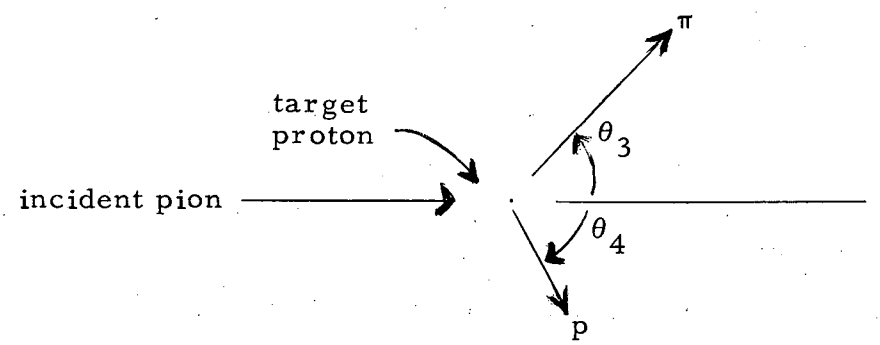

Fig. 10. Coordinate system used to describe scattering events.

In selecting elastic events, coplanarity was determined by $\Delta\phi = \pm 9$ deg for all channels. The solid angle for any given channel was determined by the pion counter π_i, the proton counter p_i being made large enough to count all possible recoil protons for a given θ_3 and $\Delta\theta_3$, and being placed at the corresponding θ_4.

Table I lists the following for all thirteen π_i: R, θ_3, the counter width $\Delta\theta_3$, and the center-of-mass solid angle subtended at each of the five energies of the experiment. Because of the small dimensions of the target as compared with the distance from it to any scintillation counter, a particle scattering in the front or back of the target vessel saw almost exactly the same solid angle as a particle scattering in the center. Therefore, the solid angle was calculated from the center of the hydrogen target, and contained a probable error of less than 1% for particles scattering in different parts of the target.

Figure 11 is a photograph of the counter arrangement showing the pion counters to the right, and the proton counters to the left, of the beam line.

Counters M_1 and M_2 monitored the pion beam incident on the hydrogen target. Counter M_1 was large enough to count all the pions in the beam, whereas M_2, a 1-1/2-in.-diam counter, was positioned before the hydrogen target in such a way as to eliminate from consideration any particle that might scrape the side walls of the target vessel.

S_0 was placed close to the target and out of the main beam, and between the hydrogen target and the pion counters. This was to ensure that all the acceptable scattering events originated at the hydrogen target, and to reduce background.

The pion and proton counters were timed by placing both counters of the ith channel in the direct pion beam, and by taking delay curves between them and the monitor system. While the counters were yet in the pion beam, voltage plateaus were determined by adjusting the tube voltage to produce -4-v output pulses, as seen on a Tektronix 517A cathode-ray oscilloscope.[45] After the timing and plateauing of the counters was accomplished, we moved the counters to their final

Table I. Position, angular width, and c.m. solid angle as a function of energy, for each of the 13 channels used in the angular distribution measurement.

Channel	Counter Position θ_3 (deg)	Counter Width $\Delta\theta_3$ (deg)	c.m. solid angle (msr) T_π (Mev) = 550	600	720	900	1020
1	22	3.00	13.9	14.3	15.5	17.1	18.1
2	34	3.00	18.1	18.6	19.7	21.1	24.7
3	38	3.00	18.9	19.4	20.7	24.5	28.9
4	46	3.24	22.9	26.0	29.7	32.1	36.8
5	56	3.76	29.4	30.7	30.3	32.6	34.9
6	63	4.04	25.3	25.3	25.3	25.6	25.6
7	70	4.26	24.8	24.7	24.4	23.8	23.3
8	78	4.44	23.6	23.3	22.7	21.7	21.1
9	91	4.54	20.0	19.7	18.8	17.6	16.8
10	109	8.56	27.7	26.9	25.2	23.0	21.8
11	122	7.68	19.0	18.4	17.0	15.4	14.4
12	135	6.42	11.7	11.3	10.4	9.27	8.65
13	150	5.00	5.75	5.53	5.06	4.49	4.17

positions (Fig. 3) and inserted appropriate delays into the signal output cable. All these delays were of the order of 2 nsec.

5. Cerenkov Counter

We measured the contamination of the pion beam with a gas Cerenkov counter,[46] using sulfur hexafluoride (SF_6) gas. Measurements were taken twice during the experiment; once with the Cerenkov counter placed behind the hydrogen target position before the target itself was put in place, and later with the counter placed in front of the

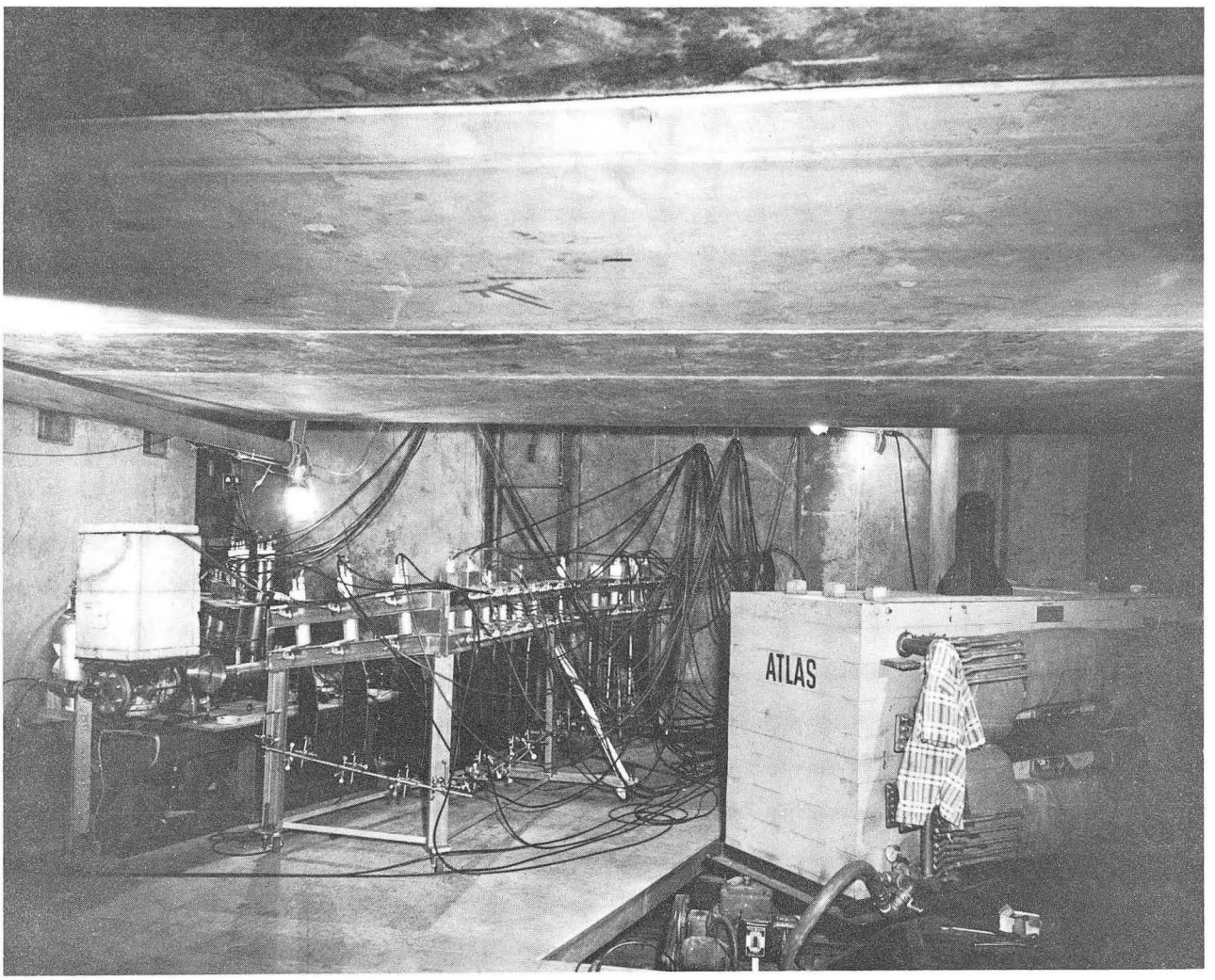

ZN-2947

Fig. 11. Picture of the scintillation counters and the Cerenkov counter in place about the hydrogen target position. The hydrogen target is not in place.

target. Figure 11 shows the Cerenkov counter in place behind the hydrogen target position, and Fig. 12 is a schematic drawing of the counter.

Two small scintillation counters, placed before and after the Cerenkov counter, were used to monitor the beam. Figure 13 is a schematic diagram of the counter arrangement and the electronics used in making these measurements.

a. Pressure curves. A typical pressure curve, taken with the counter in position behind the target, is given in Fig. 14. The monitor counters were 1 in. and 2 in. in diameter and were labeled T_1 and T_2, respectively. The Cerenkov counter was operated at a potential of 2050 volts, which gave rise to a 2 to 10% accidental background due to the large number of random noise pulses, which in turn appears as scatter of the data points.

We lowered the tube voltage on the Cerenkov counter to 1650 volts for running in front of the target. The effect of the lower voltage is to smear out the cutoff region where pions just stop radiating (the effect is the same for muons and electrons). The reason for the smearing is that a lower voltage on the phototube produces a smaller output pulse. Therefore, some real pulses are not counted because they fall just below the discriminator level of the electronics. To correct for this smearing to some extent, the voltage was raised to 1750 volts. Although the effect was not entirely eliminated, the accidental background was reduced to less than 1% at all pressures and all energies. The monitor counters here were 3 in. and 1-1/2 in. in diameter, and were labeled M_0 and M_2, respectively.

The error Δ associated with a given data point was calculated from the formula

$$\Delta = \frac{\sqrt{C(1-C/M)}}{M} , \qquad (1)$$

which is derived in Appendix C. Here we have C = number of "triples" and M = the number of "doubles" (see Fig. 13). Equation (1) is normalized by dividing Eq. (C-10) by M.

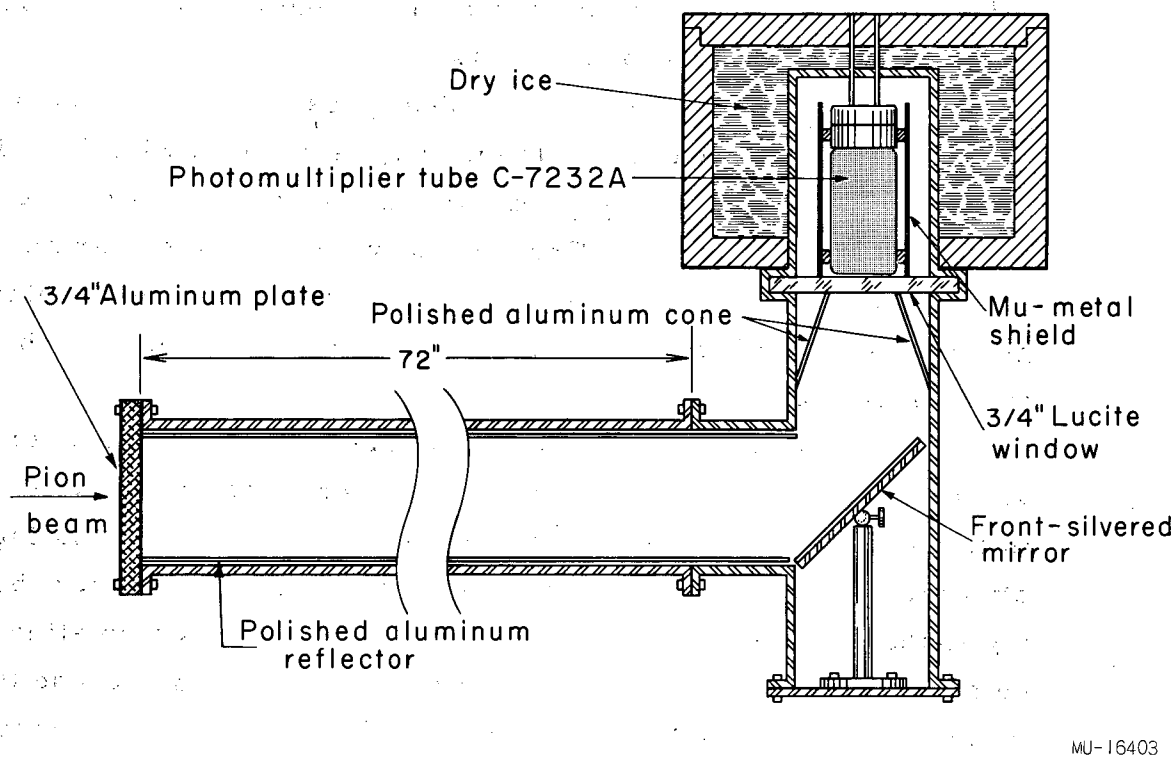

Fig. 12. Cerenkov counter.

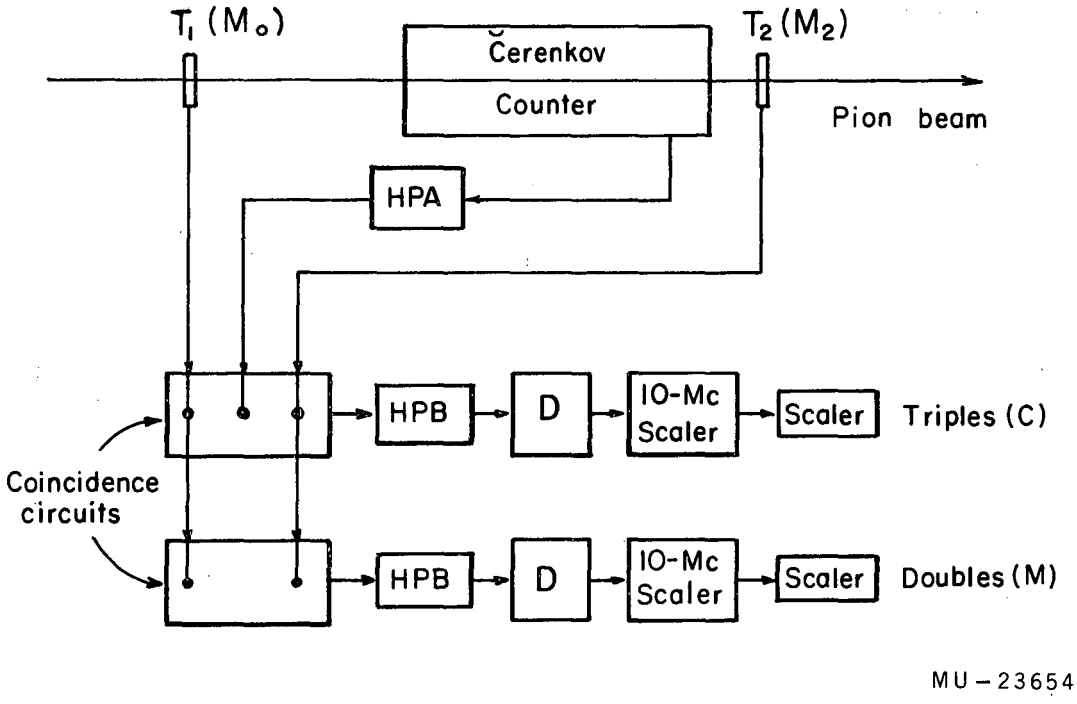

Fig. 13. Schematic diagram of the experimental arrangement and electronic components used to measure beam composition. HPA and HPB are Hewlett-Packard amplifiers, type A and B, respectively. The D are Perez-Mendez-type discriminators.

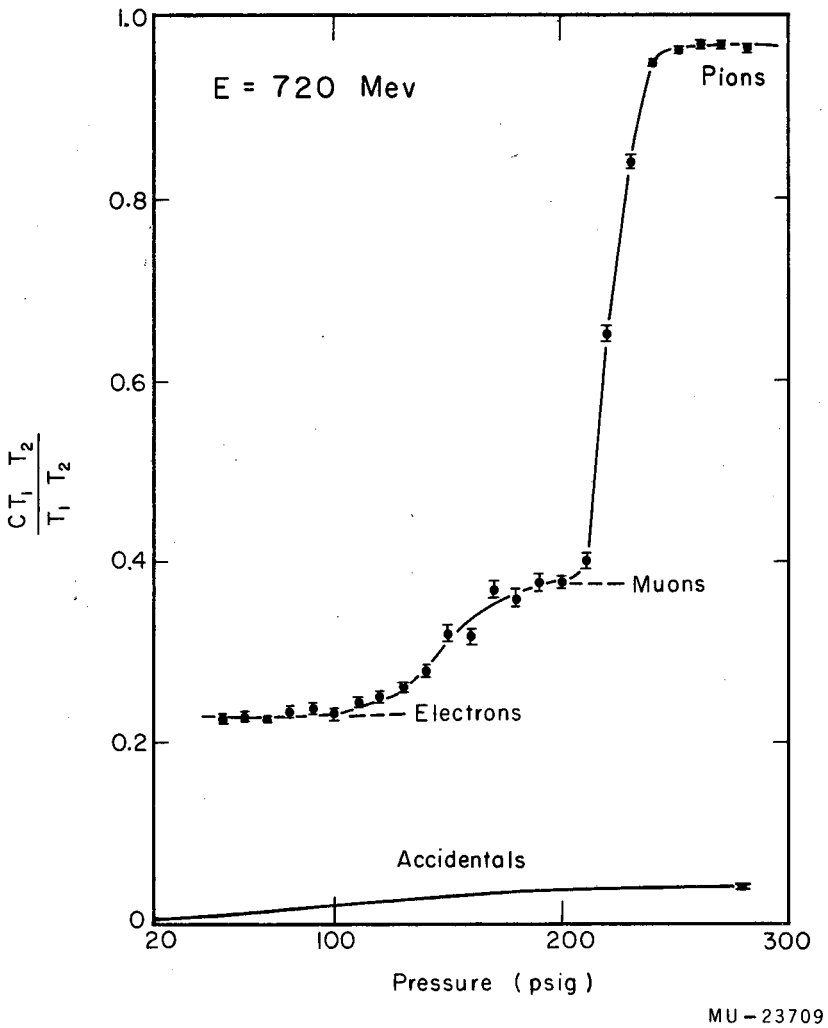

Fig. 14. Typical pressure curve taken with the Cerenkov counter behind the hydrogen target position. The tube voltage was 2050 volts.

The statistical accuracy of the points taken at this forward position was to less than 1/2% in all regions of all the curves, except at the lowest pressures (lower than thirty psig), where it increased to nearly 1%. For this reason, no error bars are shown in Figs. 15 and 16, which are typical curves taken with the counter tube voltage at 1650 and 1750 volts, respectively.

6. Electronics

Figure 17 is a block diagram of the electronics. There were thirteen sets of coincidence channels, exactly like those shown, for measuring the cross section. In addition, there were seven extra coincidence channels that were used to monitor inelastic and accidental events. To measure accidentals, a spare coincidence circuit was used with one input delayed, as shown in Fig. 17. For inelastic events, the inputs were taken from the monitor and from two counters that had no elastic kinematical relation between them (see Sec. III-B-2, Inelastics). The resolving time of the coincidence circuits was determined by the length of the "clipping line" that was used. The monitor coincidence circuits were fitted with 20-in. lines, and the Wenzel circuits used for measuring elastic events, accidentals, etc., were given 100-in. clip lines. The resolving times were thus 4 nsec and 20 nsec, respectively. The short resolving times were required of the monitor system to decrease the dead time of the circuit, because the instantaneous counting rate in the pion beam was high.

All coincidence circuits were of the Wenzel type.[47] The discriminators showing both a fast and a slow output were of the Swift-Perez-Mendez type.[48] The discriminators were used to give a slow output pulse for use in the monitor scaler, and to give a faster, shaped pulse for use in coincidence with the elastic pion-proton counter pulses. The distributed amplifiers were Hewlett-Packard models 460A and 460B. The amplifiers, and the transistorized discriminators and scalers, are described in the Lawrence Radiation Laboratory Counting Handbook.[45]

Figure 13 is a schematic diagram of the electronics used for measuring beam contamination with the Cerenkov counter.

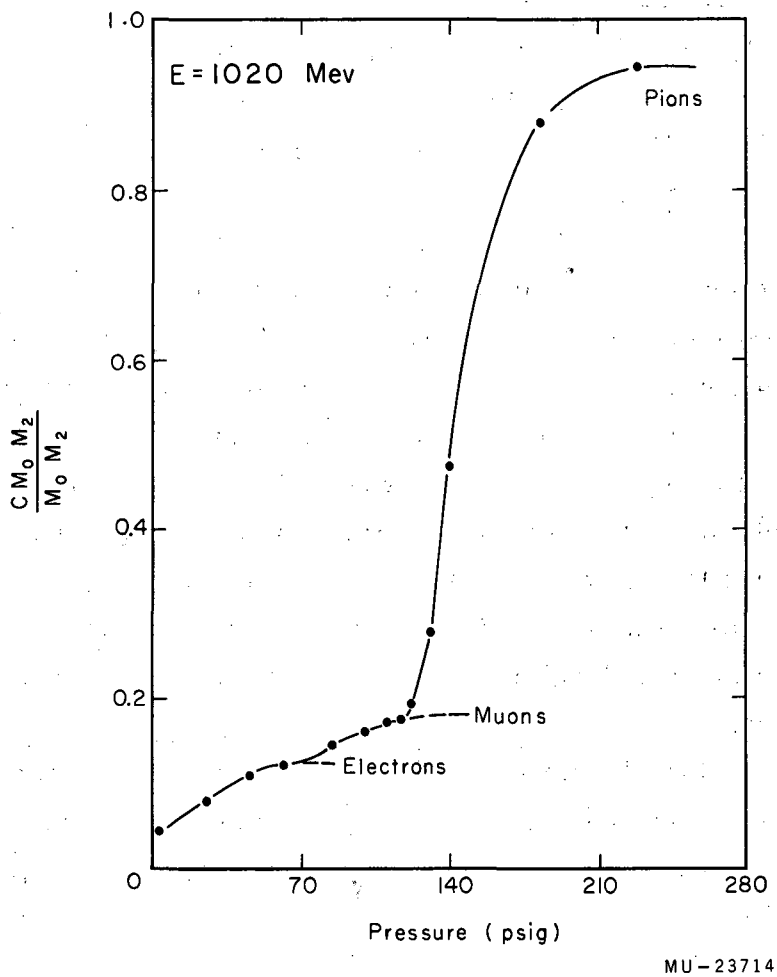

Fig. 15. Typical pressure curve taken with the Cerenkov counter in front of the hydrogen target. The tube voltage was 1650 volts.

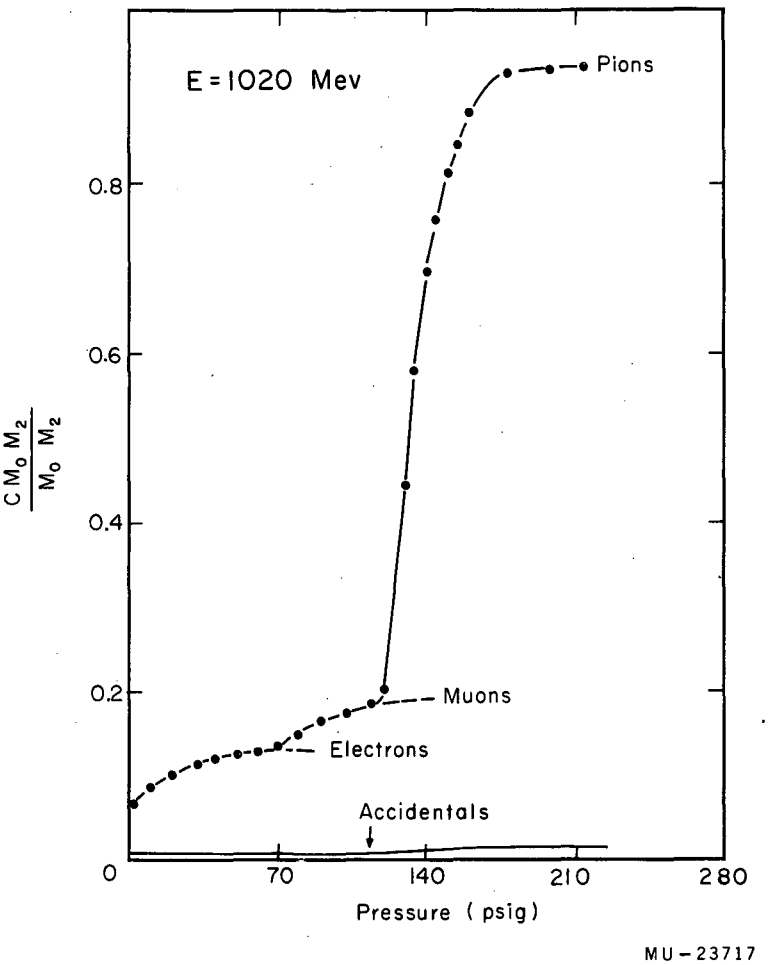

Fig. 16. Typical pressure curve taken with the Cerenkov counter in front of the hydrogen target. The tube voltage was 1750 volts.

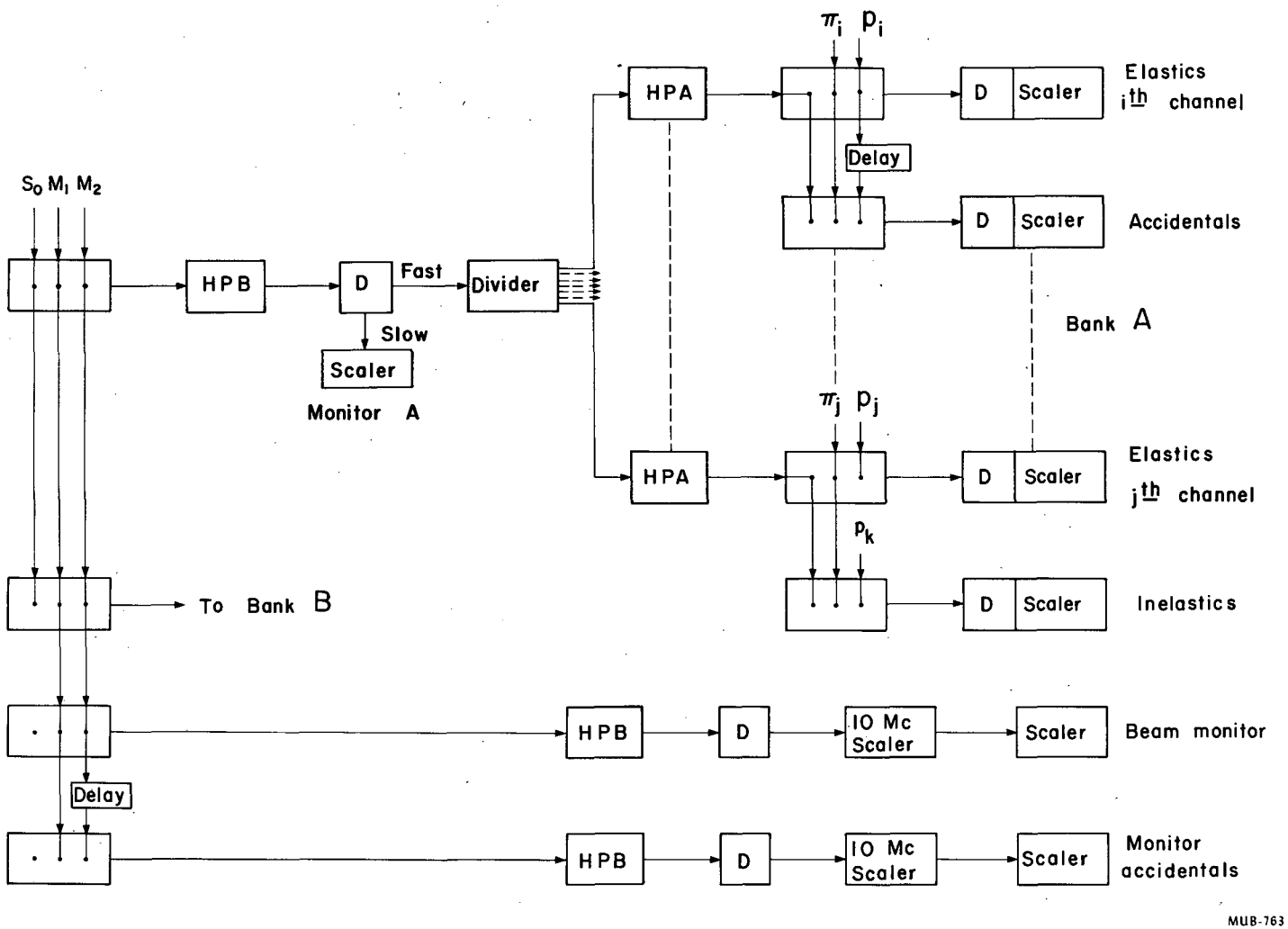

Fig. 17. Electronics block diagram. Boxes with three dots inside represent coincidence circuits. HPA and HPB stand for Hewlett-Packard amplifiers, type A and B, respectively. D stands for discriminator.

Figure 18 shows Dr. Burton J. Moyer and Dr. Victor Perez-Mendez with part of the electronics in the racks.

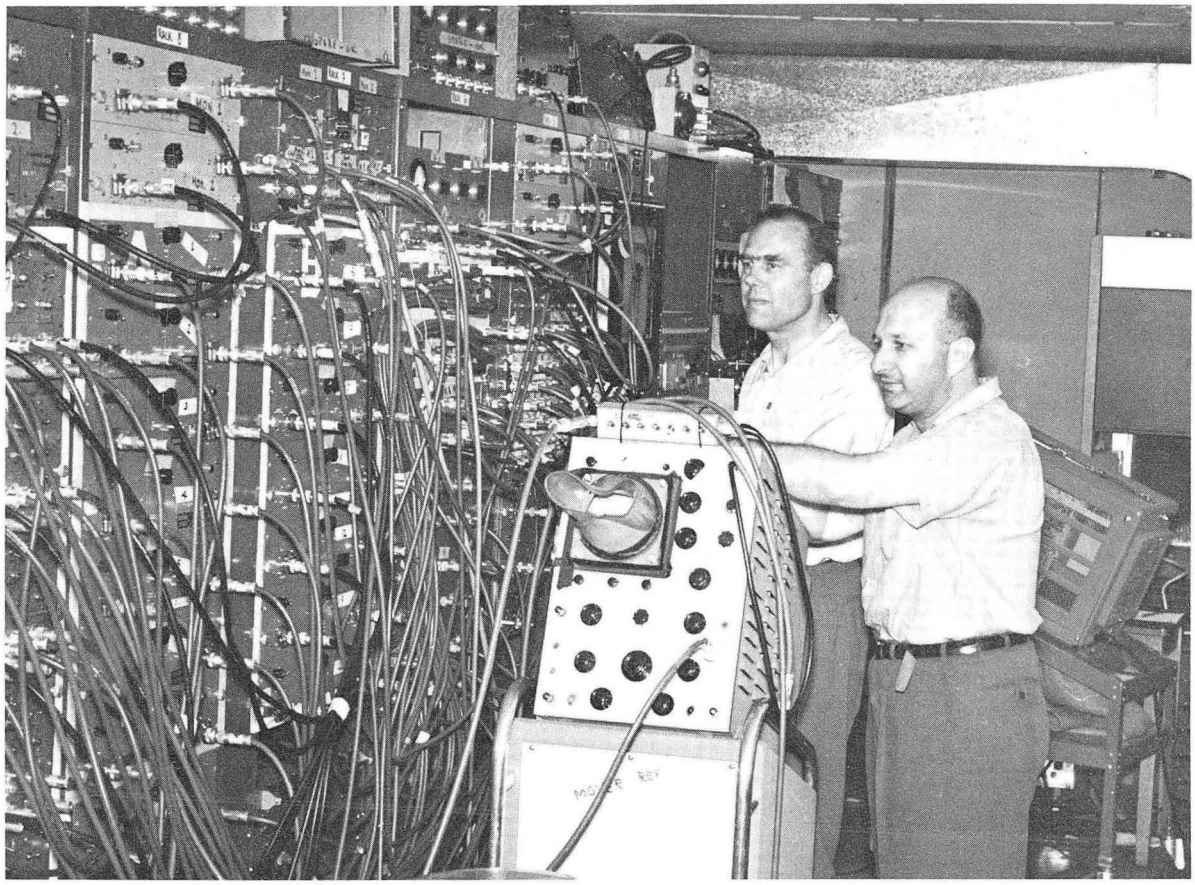

ZN-2948

Fig. 18. Dr. Burton J. Moyer and Dr. Victor Perez-Mendez, standing with part of the electronic equipment in racks.

III. ANALYSIS OF THE DATA

A. General Statistical Treatment

For a given channel, let us define the following quantities:

π_i = number of elastic coincidence counts during the ith run (the subscript i is previously used in this thesis as the channel variable),

M_i = number of counts in the pion beam monitor, and

$R_i = \pi_i / M_i$, the ratio of counts to monitor.

Then the average value of R_i, averaged over all the runs of a given type, such as target full or target empty, is

$$\bar{R} = \sum_{i=1}^{n} \pi_i \Big/ \sum_{i=1}^{n} M_i \, . \tag{2}$$

The errors associated with $\bar{R}$ and with R_i are

$$\Delta\bar{R} = \left[\frac{\sum_{i=1}^{n} M_i (R_i - \bar{R})^2}{\sum_{i=1}^{n} M_i (n-2)} \right]^{1/2} , \tag{3}$$

and

$$\Delta R = [\pi_i (1 - \pi_i / M_i)]^{1/2} / M_i \, , \tag{4}$$

respectively. Equation (4) is derived in Appendix C as the probable deviation in π_i for $\pi_i = C$ (cf. Eq. C-10). To obtain the probable deviation in R_i, Eq. C-10 must be divided by M_i. Equation (4) is exact for $\pi_i \approx M_i$, but for this experiment π_i is less than M_i by about six orders of magnitude, so that we can use the expression

$$\Delta R_i = [\pi_i]^{1/2} / M_i \, . \tag{5}$$

However, for $\pi_i/M_i \ll 1$ and $\pi_i \approx 1$, a more correct expression to use would be

$$\Delta R_i = [\pi_i + 1]^{1/2} / M_i . \tag{6}$$

The differential cross section is given in terms of the experimentally determined quantities by

$$\frac{d\sigma}{d\Omega^*} = \frac{1}{nx\Omega^*} \left[\overline{R}_{full} - \overline{R}_{empty} \right] , \tag{7}$$

where n = number of nuclei per unit volume, x = target length, and Ω^* = the center-of-mass solid angle of the channel. Corrections to this expression are discussed in subsequent sections.

The statistical error associated with $d\sigma/d\Omega^*$ is

$$\Delta\left(\frac{d\sigma}{d\Omega^*}\right) = C \left\{ \left[\frac{\sum_{i=1}^{n} \pi_i}{\left(\sum_{i=1}^{n} M_i \right)^2} \right]_{full} + \left[\frac{\sum_{i=1}^{n} \pi_i}{\left(\sum_{i=1}^{n} M_i \right)^2} \right]_{empty} \right\}^{1/2} \tag{8}$$

in analogy to Eq. (5), and where

$$C = 1/nx\Omega^* . \tag{9}$$

The error based upon the reproducibility of repeated runs is given by

$$D = C \left[\Delta\overline{R}^2_{full} + \Delta\overline{R}^2_{empty} \right]^{1/2} . \tag{10}$$

The residue is

$$Res_i = R_i - \overline{R} . \tag{11}$$

Only internally consistent R_i's were combined to derive the differential cross section. To test consistency, we used a criterion similar to the statistical criterion of Rossini and Deming,[49] who require that the plot of each point plus two standard deviations overlap the plot of the mean plus two standard deviations of the mean.

Since a heavily weighted run lying far from the mean could greatly influence the mean and move the two close together, we defined the following quantities:

$$\bar{R}_j = \sum_{i \neq j} \pi_i \Big/ \sum_{i \neq j} M_i \,, \tag{12}$$

the average ratio of counts-to-monitor, without the run in question; and

$$\Delta\bar{R}_j = \left[\frac{\sum_{i \neq j} M_i (R_i - \bar{R}_j)^2}{\sum_{i \neq j} M_i (n-2)} \right]^{1/2} , \tag{13}$$

the error associated with $\bar{R}_j$; and

$$\mathrm{Res}_j = R_j - \bar{R}_j \,, \tag{14}$$

the residue, where the mean is not now influeced by the run in question.

We now use

$$|\mathrm{Res}_j| > 3(\Delta R_j + \Delta\bar{R}_j) \tag{15}$$

as the criterion for rejecting inconsistent runs. The ΔR_j used in Eq. (15) is the one defined in Eq. (6).

Less than 1% of the data was rejected on the basis of this criterion.

B. Corrections to the Data

1. Accidentals

Accidentals due to the ambient background of particles inside the concrete shielding house were measured and found to give a correction to the data of less than 0.1%.

If two beam particles came down the channel together in time (i.e., within the resolving time of the monitor coincidence circuit), our beam monitor would not separate them, but the probability of an elastic scatter would be doubled, and there would also be a greater possibility that an inelastic event would appearing as an elastic one. This type of accidental event was not detectable by our monitor system, but would have an effect on the normalization of the cross section.

The probability of two beam particles appearing together in time increases with the rf structure from the Bevatron. We discuss this further in Sec. III-B-8 (Normalization).

2. Inelastics

This correction is made by a simple subtraction from the measured elastic cross section. Expressed mathematically, we have

$$\frac{d\sigma}{d\Omega^*} = C(A - B), \tag{16}$$

where C is the constant defined in Eq. (9), A is equal to the average ratio of counts-to-monitor, target full minus target empty, and B is the inelastics correction. If we use this notation, we could write Eq. (7) as

$$\frac{d\sigma}{d\Omega^*} = CA. \tag{17}$$

The rest of this section is concerned with the determination of B in Eq. (16).

Figure 19 shows a plot of proton angle vs pion angle in the laboratory system at 900 Mev. Other energies are similar. The heavy solid line represents elastic events, and the area between the heavy dashed lines represents elastic events as seen by pairs of counters having finite angular width. The combination of a pion and proton counter in coincidence is represented by a single point on this graph. The solid and dashed fine lines represent "reverse elastic" events in which the pion registers in the proton counter and vice versa; these events are discussed in detail in the next section. Inelastic events were measured by selecting counter pairs whose points lie outside the region of elastic and reverse elastic events in this figure.

If the value for the inelastics determined by such a pair were plotted as the height above this graph at that point, the background of inelastics would appear as a three-dimensional surface lying above the plane of the figure. This surface will peak more toward small angles for both kinds of particles at successively higher energies.

The problem of determining the inelastics background may then be thought of as the problem of mapping this surface. Interpolation along the surface gives the value for the background correction in the region of elastic events. A straight-line interpolation was made because the distribution of inelastic events was not sufficiently well determined in this experiment to warrant the use of a less simple function.

Because the inelastics correction is not well known, we have neglected the correlation between particles in inelastic events. Also, because of this uncertainty, the errors on the points of the differential cross section curve were increased by at least a factor of 10% in every case, and by as much as a factor of four in the region of very small elastic cross section. However, because the greatest uncertainty occurs for very small values of the cross section, the shape of the differential curves is not materially changed.

3. Reverse Elastics

In Fig. 19, the reverse elastic events are represented by the solid and dashed fine lines. Only a few channels are affected by the presence of reverse elastics.

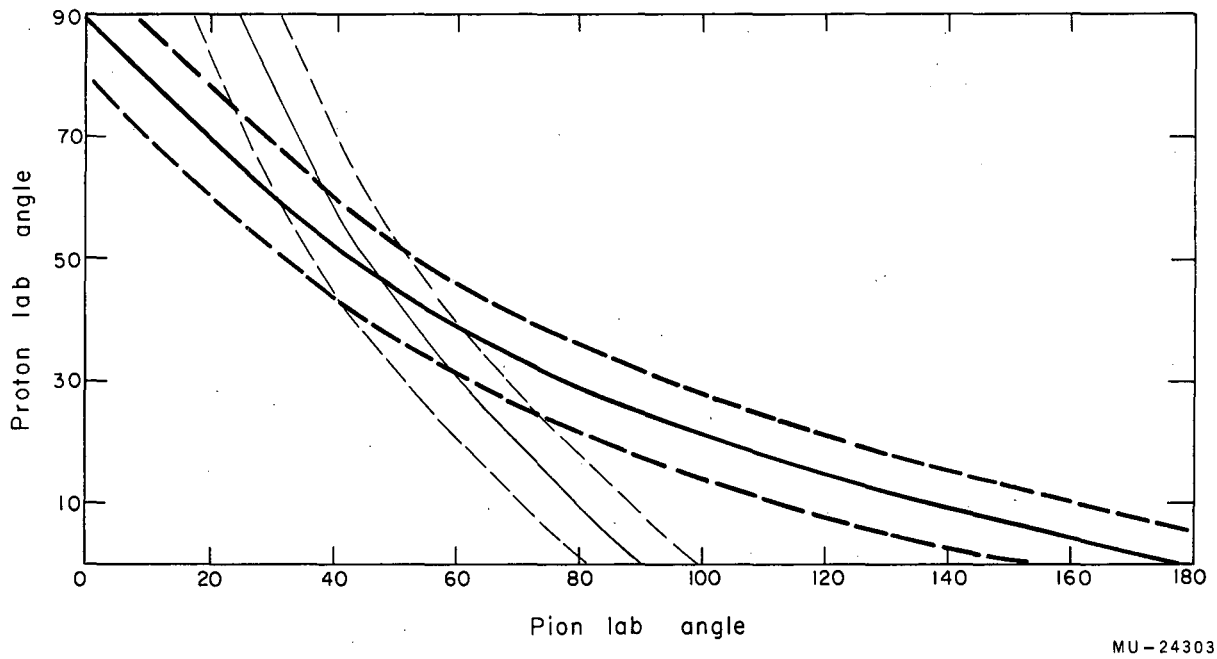

Fig. 19. Pion lab angle vs proton lab angle at 900 Mev. The heavy solid line represents the kinematical combinations of angles for elastic events. The area between the heavy dashed lines represents elastic events as seen by counters having finite angular width. The solid and dashed fine lines represent "reverse elastic" events in which the pion registers in the proton counter and vice versa.

If we call the reverse elastics correction E, we can write

$$\frac{d\sigma}{d\Omega^*} = CE(A-B), \qquad (18)$$

to replace Eq. (16).

This correction is twofold: first, a simple geometrical correction; and second, a time-of-flight correction because the pion and proton counters were not the same distance from the hydrogen target, and because the two kinds of particles have different velocities. When the pion counts in the proton counter and vice versa, we have a situation in which the faster particle (pion) travels about one-half as far and the slower particle (proton) about twice as far, as they would in the planned situation for true elastic events. This means that the counter pulses, which would have arrived at the coincidence circuit at the same time, are instead shifted apart in time, affecting the efficiency of the coincidence circuit according to the deviation from the timing curve for "real" elastics. This latter correction introduced essentially all the uncertainty in the reverse elastics correction.

Channels 2 through 5 were the ones generally affected by this correction, and so the errors on the points in this region are much larger than those due to statistics alone. The constant E in Eq. (18) ranged in value from 0.64 to 0.99.

4. Beam Composition

The three main constituents of the negative beam were electrons, muons, and pions.

a. Pions, Muons, and Electrons. Figures 20 and 21 show the muon and electron contamination of the pion beam as a function of energy, for the Cerenkov counter arrangement behind and in front of the hydrogen target, respectively. The large errors in these figures result mainly from the uncertainty in determining the precise value for the muon and electron "plateaus."

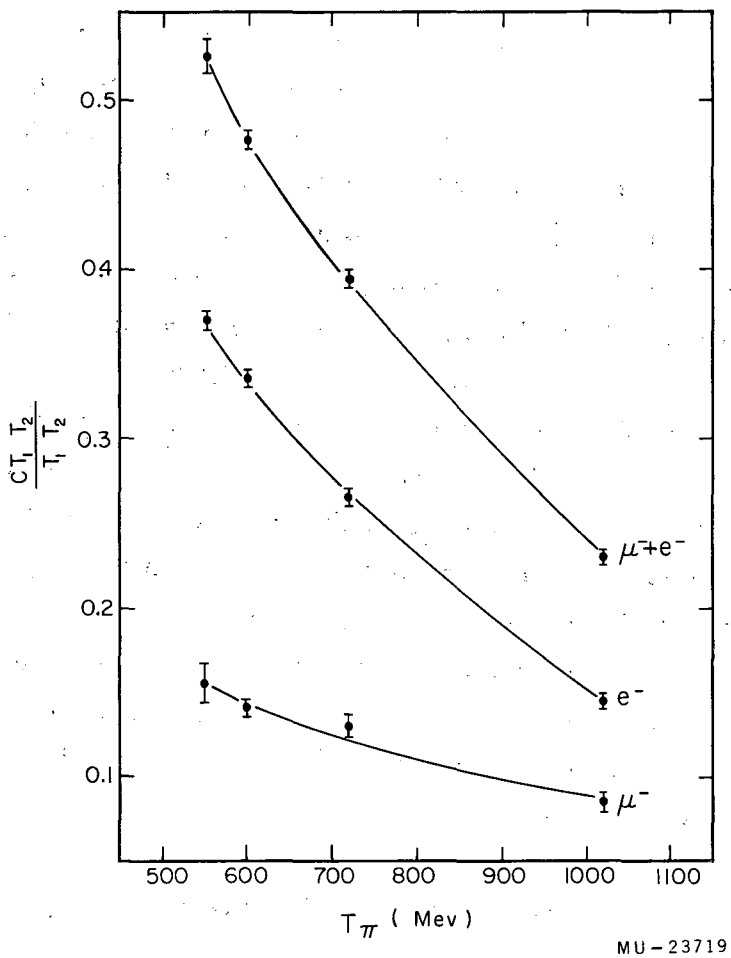

Fig. 20. Muon and electron contamination of the pion beam as a function of energy, measured downstream from the hydrogen target position.

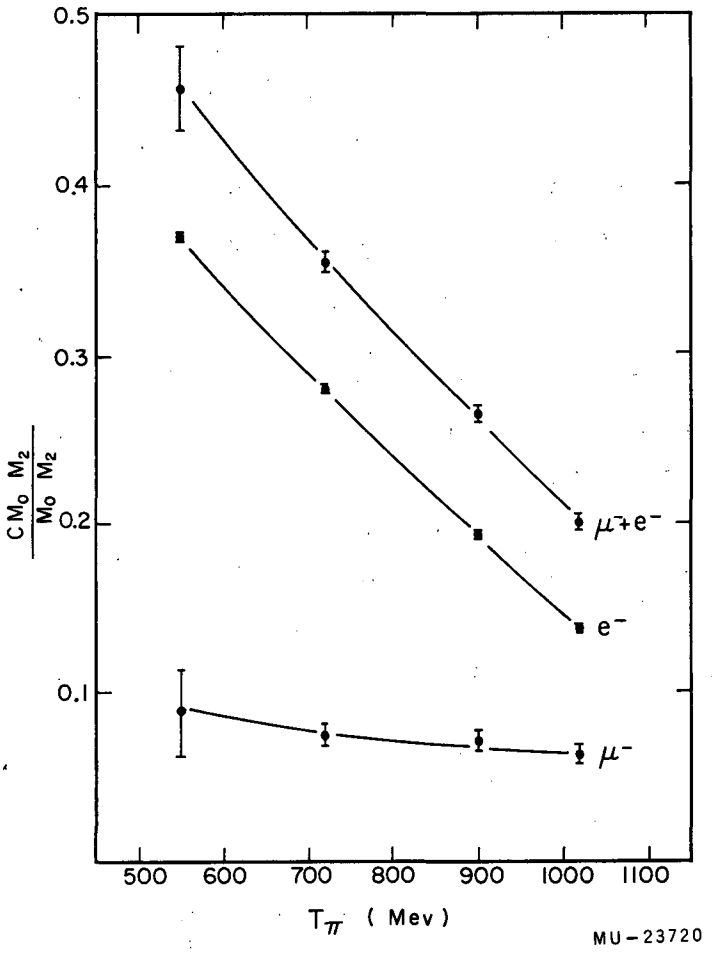

Fig. 21. Muon and electron contamination of the pion beam as a function of energy, measured upstream from the hydrogen target.

To determine the amount of muon contamination at the hydrogen target position, we made a linear interpolation between the values obtained in the two positions of the Cerenkov counter. The value of the muon contamination is higher downstream because muons are constantly being added to the beam from pion decays, so that the numbers of both pions and muons are continually changing as the beam moves along. The electron contamination did not vary appreciably from one position to the other, since the main source of electrons is the primary target inside the Bevatron, so we used, as the values at the hydrogen target, the values obtained from the forward position of the Cerenkov counter, which had a higher statistical accuracy associated with them.

The large number of electrons was present because the pions were produced in the Bevatron target at angles of less than 4 deg with respect to the direction of the circulating proton beam, so that decay γ rays from the π^0 mesons produced near the front of the target had to pass through about three radiation lengths of copper before emerging from the target material. Hence many gammas were converted to electron-positron pairs, in which the electron had the right momentum to pass through our magnet system and be counted in the monitor system.

Since neither electrons nor muons interact strongly with the target nucleons, their sole effect is contained in the over-all normalization of the differential cross-section angular distribution curves.[50]

b. Other Particles. The presence in the beam of negatively charged particles of mass greater than that of the pion can be neglected. In the energy region of this experiment, the cross sections for producing K^- particles, antiprotons, and π^-'s in the primary target were in the ratio of $(0.74 - 0.87) \times 10^{-3} / (0.64 - 1) \times 10^{-5} / 1$, respectively.[51]

The three main constituents of the negative beam were therefore electrons, muons, and pions.

5. Coulomb Scattering

The mean scattering angle for multiple Coulomb scattering in the worst case was 0.16 deg as compared with about 1 deg for the angular divergence of the beam at the hydrogen target. The channel

nearest to the beam was at 22 deg in the laboratory system, so no Coulomb correction was necessary.

6. Angular Width of the Scintillation Counters

The effect of finite counter width need be considered only in the regions of the differential cross-section curve where the second derivative of the curve is large. In this experiment this correction is quite small, being of the order of 0.1% to 1.0%.

7. Particle Rescattering

This effect is very small except in the region where the scattered particles have very low energy. For protons scattered near 90 deg from the incident beam direction, the energy is so low that many of them cannot escape the hydrogen target. In all such cases, the point in question was eliminated from the differential cross-section curve. For example, at 600 Mev, channel 1, for which the proton counter was placed at an angle θ = 71 deg in the laboratory system, was not used in determining the angular distribution.

8. Normalization

Because we were unable to determine an absolute normalization for the data of this experiment, we normalized the data to the total elastic cross sections as determined by many workers and summarized by Brisson et al.[7] and Shonle.[29] Figure 22 shows their data and the curve we drew and used for the normalization.

In normalizing our data, we treated the dispersion relations point at $\cos\theta_3^* = 1.0$ as a known, fixed point and varied the experimental points together to arrive at the desired value of the total elastic cross section. The point at $\cos\theta_3^* = 1.0$ and listed in Table II for the five energies of this experiment was determined from dispersion relations and the optical theorem,[52] using Devlin's final total cross section data[8] for the imaginary part of the dispersion integral.

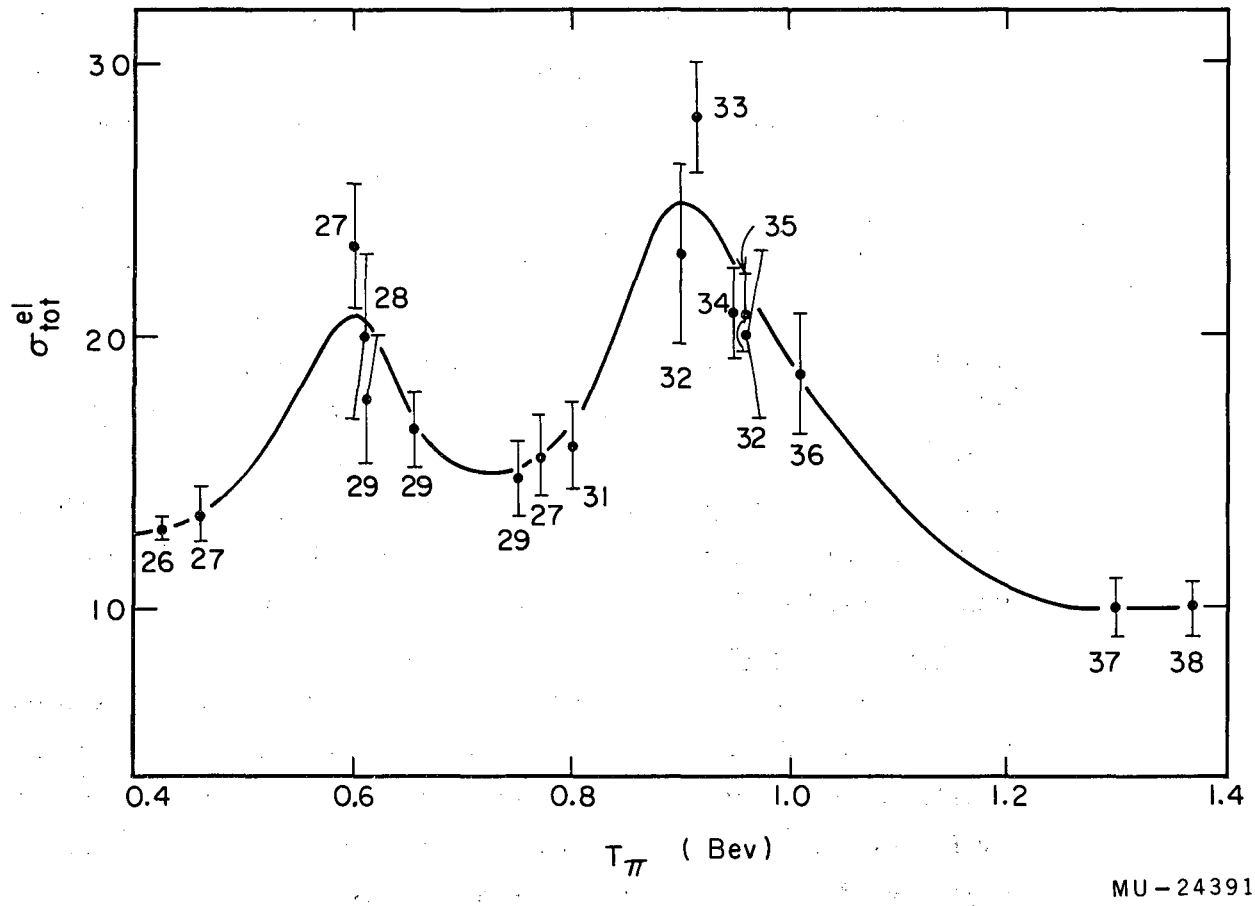

Fig. 22. Total cross section for elastic π^--p scattering as a function of incident pion kinetic energy. The numbers on the graph correspond to numbers in the reference section of this thesis.

Table II. Value of the differential cross section at $\cos\theta_3^* = 1.0$ as determined from dispersion relations and the optical theorem, at the five energies of this experiment.

Energy (Mev)	$\frac{d\sigma}{d\Omega^*}(0)$ (mb/sr)
550	5.37 ± 0.21
600	7.05 ± 0.26
720	6.74 ± 0.24
900	17.83 ± 0.52
1020	13.16 ± 0.38

There are several phenomena that could be responsible for the normalization difficulties:

(a) The Swift-Perez-Mendez discriminators were rated at 10 Mc for evenly spaced pulses.[48] This means that there is a dead time of 10^{-7} sec associated with each signal pulse handled by the discriminator. Our average counting rate was often as high as 5×10^4 pions per 100-msec pulse, or 5×10^5 pions per second. Therefore, for 5% of the time, the discriminator was unable to handle any pulses. For pulses randomly distributed in time, this means that about 5% of them will not be counted. If the rating of the discriminators is good to within a factor of two, then the uncertainty in the normalization from this source will be about 5%.

(b) Any bunching of the rf structure in the beam spill would increase the uncertainty mentioned above by increasing the instantaneous counting rate. As we mentioned in Sec. II-B-1-a (Pion Source-Beam Spill Effects), there was considerable rf structure apparent in the pion beam, from time to time. The amount of rf was not constant in time, so its contribution to the uncertainty could not be uniquely determined although it could have been as high as a factor of six or seven.

The shape of the angular distribution curves was reproducible, but the normalization of the curves varied by as much as 50% when the distribution at a given energy was measured at different times during the experiment.

There is another phenomenon that should be mentioned here. We used two banks of electronics in the differential cross-section measurement. Bank A contained the electronics for the first seven elastic channels, and Bank B contained the electronics for the latter six channels. Each bank had its own monitor scaler that recorded the number of particles scattered from the target and which was fed by the slow output of a Swift-Perez-Mendez discriminator (see Fig. 18 and Sec. II-B-6). Monitor A consistently counted 3 to 10% higher than Monitor B. In our normalization, we normalized the elastic channels in Bank A to Monitor A and those in Bank B to Monitor B.

IV. EXPERIMENTAL RESULTS

A. Data

The differential cross sections determined by this experiment for elastic π^--p scattering at 550, 600, 720, 900, and 1020 Mev are listed in Table III and plotted in Figs. 23 through 27. These curves include all the important corrections discussed in the preceding sections. The points at $\cos \theta_3^* = 1.0$ were determined from dispersion relations (see Table II).

B. Curve Fitting

We made a least-squares fit of a cosine power series to the differential cross section data of this experiment:

$$\frac{d\sigma}{d\Omega^*} = \sum_{k=0}^{n} a_k \cos^k \theta_3^* . \tag{19}$$

On the basis of a chi-squared test,[53] we were able to select the following possibilities for the n which would give the best fit: at 550 Mev, n could be 3 or 5; at 600 Mev, n could be 2 or 3; at 720 Mev, n is 5; at 900 Mev, n is again 5; and at 1020 Mev, n could be either 5 or 6. Figure 28 shows a plot of the goodness-of-fit parameter $[\chi^2/d']^{1/2}$. Here d' is equal to the number of degrees of freedom:

$$d' = p - (n + 1) - 1, \tag{20}$$

where p is the number of data points, n + 1 is the number of coefficients determined in an nth order fit, and the final 1 comes from the fact that we used the dispersion relations point at zero degrees to obtain our normalization (see Sec. III-B-8, Normalization) and in the curve fitting, but did not determine it in this experiment.

Table III. Differential cross section for $\pi^- + p \rightarrow \pi^- + p$ as a function of the cosine of the pion scattering angle in the c.m. system at incident pion kinetic energies of 550, 600, 720, 900, and 1020 Mev.

T = 550 Mev		T = 600 Mev		T = 720 Mev		T = 900 Mev		T = 1020 Mev	
$\cos\theta_3^*$	$d\sigma/d\Omega^*$ (mb/sr)	$\cos\theta_3^*$	$d\sigma/d\Omega^*$ (mb/sr)	$\cos\theta_3^*$	$d\sigma/d\Omega^*$ (mb/sr)	$\cos\theta_3^*$	$d\sigma/d\Omega^*$ (mb/sr)	$\cos\theta_3^*$	$d\sigma/d\Omega^*$ (mb/sr)
1.000	5.37±0.21	1.000	7.05±0.26	1.000	6.74±0.24	1.000	17.83±0.52	1.000	13.16±0.38
0.621	2.62±0.20	0.608	3.09±0.11	0.577	1.329±0.086	0.782	4.633±0.068	0.766	3.546±0.087
0.542	2.15±0.14	0.527	2.625±0.089	0.492	1.058±0.075	0.534	0.345±0.034	0.506	0.254±0.038
0.377	1.59±0.19	0.359	1.43±0.33	0.318	0.58±0.22	0.443	0.104±0.039	0.412	0.098±0.049
0.168	0.91±0.23	0.148	0.65±0.15	0.102	0.53±0.10	0.260	0.099±0.079	0.224	0.086±0.060
0.027	0.497±0.098	0.006	0.268±0.071	-0.041	0.212±0.071	0.039	0.144±0.036	0.001	0.210±0.037
-0.107	0.203±0.098	-0.128	0.067±0.071	-0.174	0.219±0.071	-0.103	0.228±0.042	-0.141	0.221±0.064
-0.249	0.070±0.097	-0.269	0.015±0.081	-0.312	0.332±0.082	-0.234	0.369±0.041	-0.270	0.285±0.057
-0.451	0.142±0.091	-0.467	0.184±0.072	-0.503	0.701±0.069	-0.367	0.697±0.043	-0.400	0.343±0.059
-0.669	0.602±0.094	-0.681	0.702±0.085	-0.705	1.061±0.063	-0.549	1.548±0.050	-0.575	0.766±0.059
-0.787	1.136±0.087	-0.795	1.017±0.082	-0.812	1.045±0.053	-0.735	2.367±0.053	-0.752	1.41±0.15
-0.876	1.458±0.084	-0.880	1.40±0.13	-0.891	0.963±0.052	-0.832	2.346±0.060	-0.843	1.181±0.057
-0.946	1.63±0.16	-0.948	1.538±0.096	-0.953	0.554±0.067	-0.903	1.924±0.059	-0.910	0.940±0.057
						-0.958	0.958±0.060	-0.961	0.376±0.051

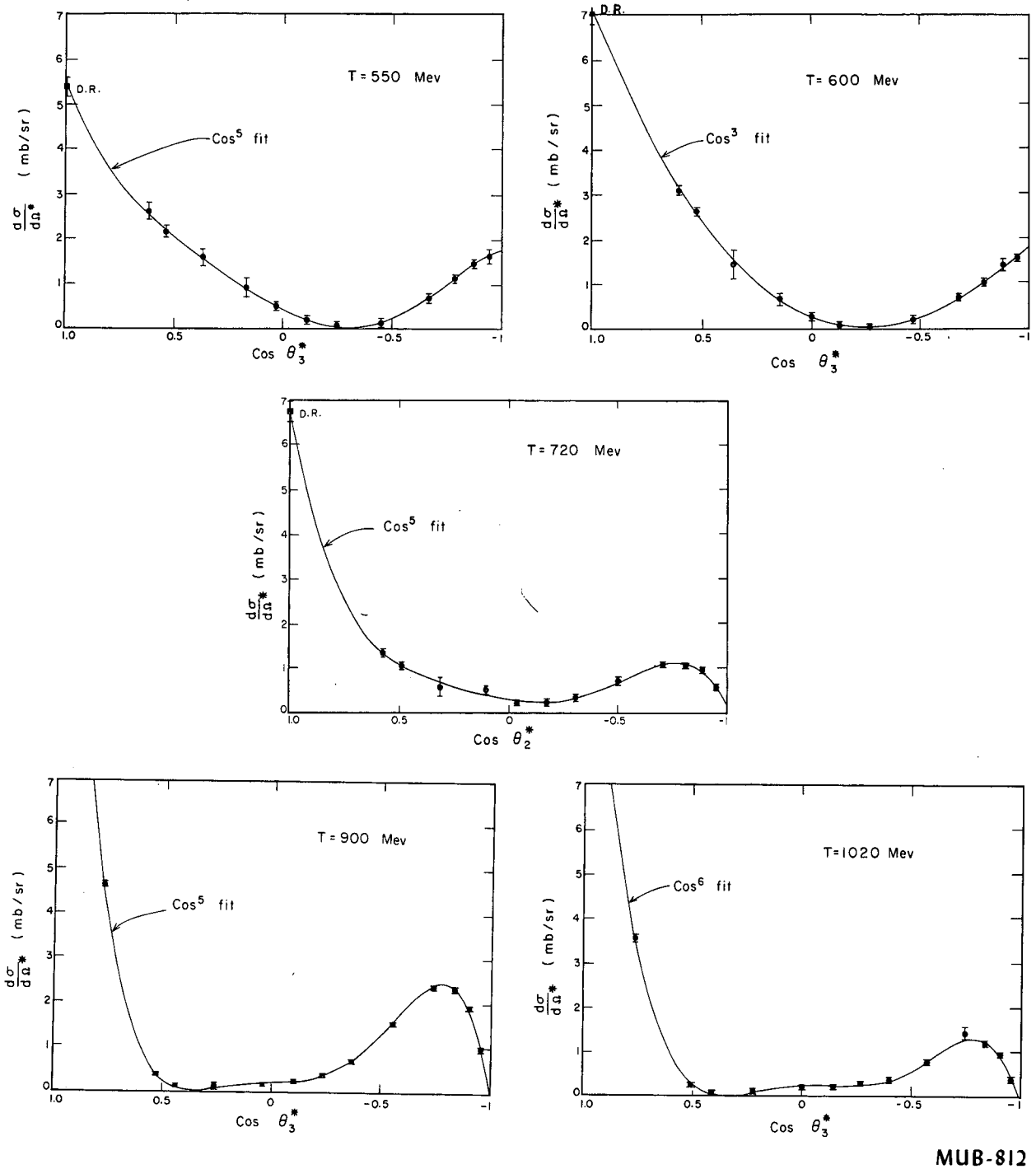

Figs. 23-27. Differential cross section for $\pi^- + p \rightarrow \pi^- + p$ as a function of the cosine of the pion scattering angle in the center-of-mass system at an incident pion kinetic energy of 550 Mev (Fig. 23); of 600 Mev (Fig. 24); of 720 Mev (Fig. 25); of 900 Mev (Fig. 26); and of 1020 Mev (Fig. 27). The error bars associated with the data points include systematic as well as statistical errors.

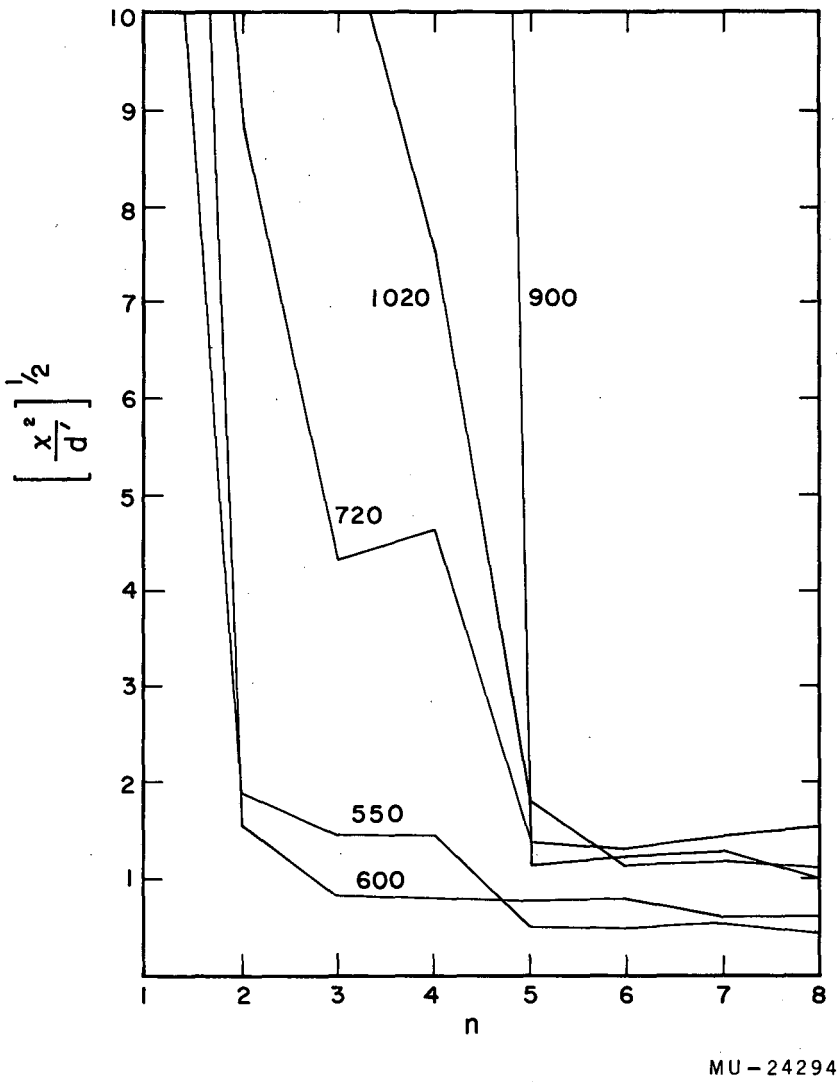

Fig. 28. Goodness-of-fit parameter as a function of the order of the fit.

To remove the ambiguity as to which n gives the best fit at 550, 600, and 1020 Mev, we applied a Fisher test,[53] which tests the probability that the coefficient $a_n \neq 0$, for successive values of n. On the basis of both tests used together, we were able to fix the best fit n as: 5 for 550 Mev; 3 for 600 Mev; and 6 for 1020 Mev. The Fisher test corroborates the selection of 5 as the value of n for a best fit at 720 and 900 Mev.

Table IV gives the values of a_k as determined by fitting these data, as well as those determined by others,[26, 29, 33, 54] in the energy range 230 through 1300 Mev. The a_k appear plotted in Figs. 29 through 31.

In the next section I discuss the behavior of the coefficients a_k as a function of energy, and the possible partial waves contributing to the "resonance" phenomena.

In making the χ^2 and Fisher tests, only random errors were used with the data. The curve fitting was done using the same data, but with larger errors, combining systematic errors with the random errors. This was done because the χ^2 test measures the probability that a purely random distribution gives no better fit, and the Fisher test depends upon the values of χ^2.

Table IV. Coefficients a_k from the expansion of the differential cross section angular distributions in a cosine power series.

T_T (Mev)	Coefficients (mb/sr)						
	a_0	a_1	a_2	a_3	a_4	a_5	a_6
230[a]	0.91 ± 0.04	0.55 ± 0.14	2.63 ± 0.36	-0.02 ± 0.25	-0.66 ± 0.45	-	-
290[a]	0.76 ± 0.03	0.84 ± 0.09	0.72 ± 0.21	-0.69 ± 0.16	0.47 ± 0.27	-	-
370[a]	0.66 ± 0.03	1.03 ± 0.11	0.89 ± 0.25	-1.56 ± 0.51	-0.45 ± 0.32	0.81 ± 0.52	-
427[a, c]	0.75 ± 0.06	1.62 ± 0.22	0.84 ± 0.40	-3.02 ± 0.74	0.05 ± 0.44	1.91 ± 0.63	-
550[b]	0.43 ± 0.07	2.38 ± 0.32	2.71 ± 0.44	-2.91 ± 1.33	0.45 ± 0.45	2.32 ± 1.12	-
600[b]	0.26 ± 0.04	1.95 ± 0.13	4.19 ± 0.13	0.68 ± 0.22	-	-	-
610[c]	0.26 ± 0.05	1.83 ± 0.32	3.92 ± 0.67	0.31 ± 0.52	-1.12 ± 0.78	-	-
655[c]	0.26 ± 0.04	1.48 ± 0.20	4.31 ± 0.50	0.37 ± 0.35	-2.29 ± 0.56	-	-
720[b]	0.30 ± 0.05	0.77 ± 0.23	1.95 ± 0.32	-2.70 ± 0.92	1.21 ± 0.33	5.20 ± 0.75	-
750[c]	0.27 ± 0.05	0.77 ± 0.20	2.09 ± 0.47	-3.73 ± 1.06	1.02 ± 0.73	6.48 ± 1.31	-
900[b]	0.18 ± 0.03	-0.19 ± 0.11	0.10 ± 0.20	-7.78 ± 0.53	8.80 ± 0.30	16.97 ± 0.55	-
915[d]	0.21 ± 0.04	0.71 ± 0.18	0.40 ± 0.35	-3.07 ± 0.97	6.10 ± 0.44	10.35 ± 0.95	-
1020[b]	0.22 ± 0.03	-0.19 ± 0.13	-1.91 ± 0.38	-2.98 ± 0.63	11.46 ± 1.21	9.87 ± 0.65	-3.28 ± 0.95
1300[e]	0.24 ± 0.06	-0.58 ± 0.22	-0.95 ± 0.49	1.05 ± 1.14	4.42 ± 0.76	2.86 ± 1.30	-

[a] Lester K. Goodwin (Ref. 54).

[b] Data of this experiment.

[c] John I. Shonle (Ref. 29).

[d] S. Bergia et al. (Ref. 33).

[e] M. Chrétien et al. (Ref. 37).

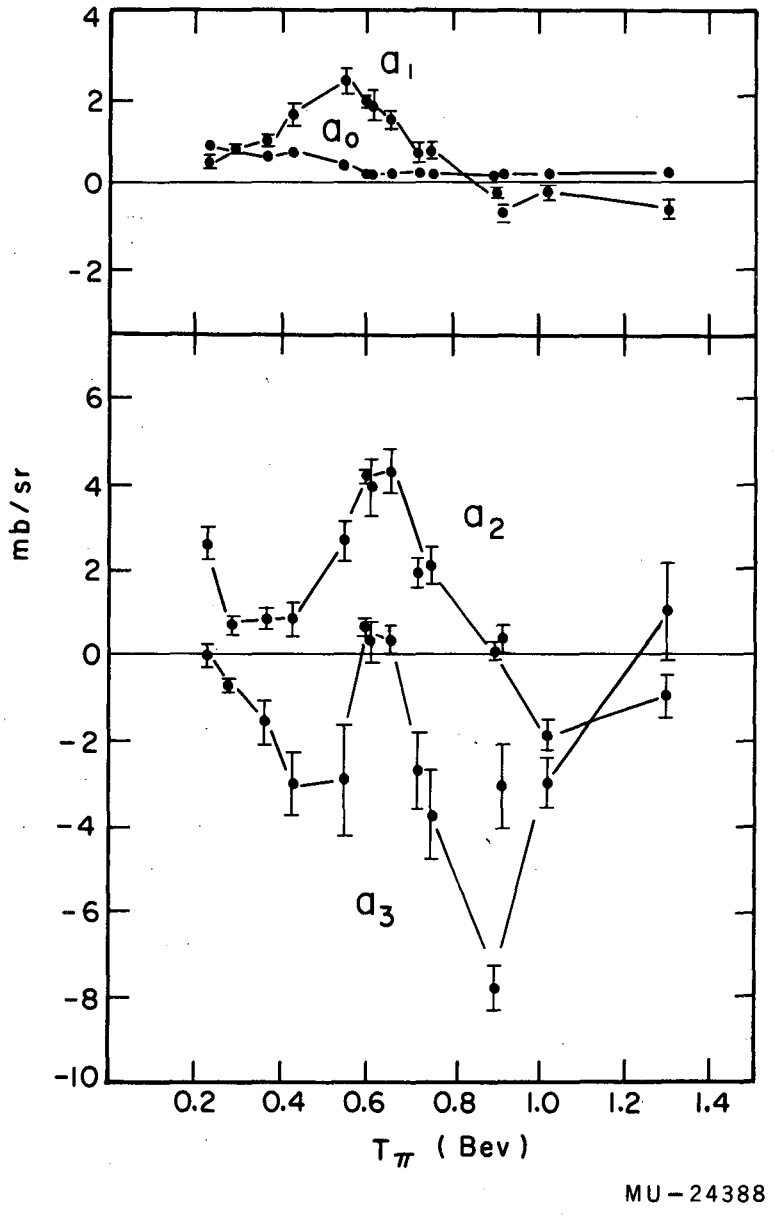

Fig. 29. Coefficients a_0, a_1, a_2, a_3 in the cosine power series expansion of the angular distribution from $\pi^- + p \rightarrow \pi^- + p$ as a function of incident pion kinetic energy.

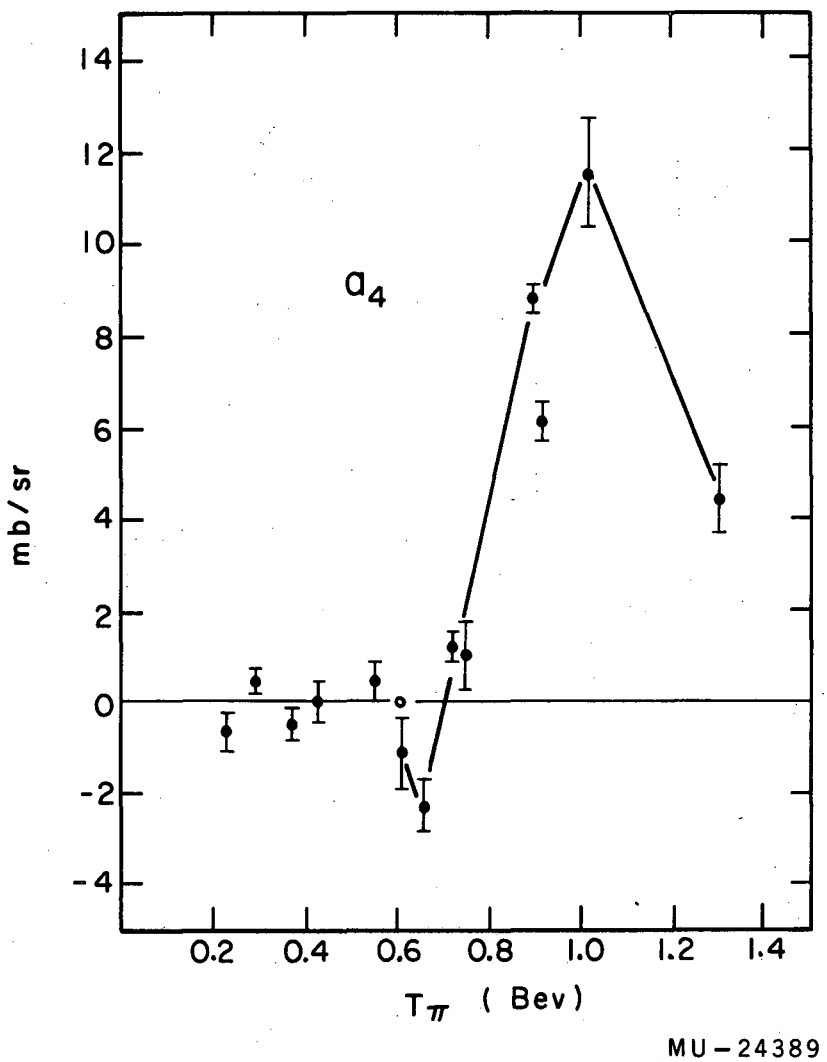

Fig. 30. Coefficient a_4 in the cosine power series expansion of the angular distribution from $\pi^- + p \rightarrow \pi^- + p$ as a function of incident pion kinetic energy.

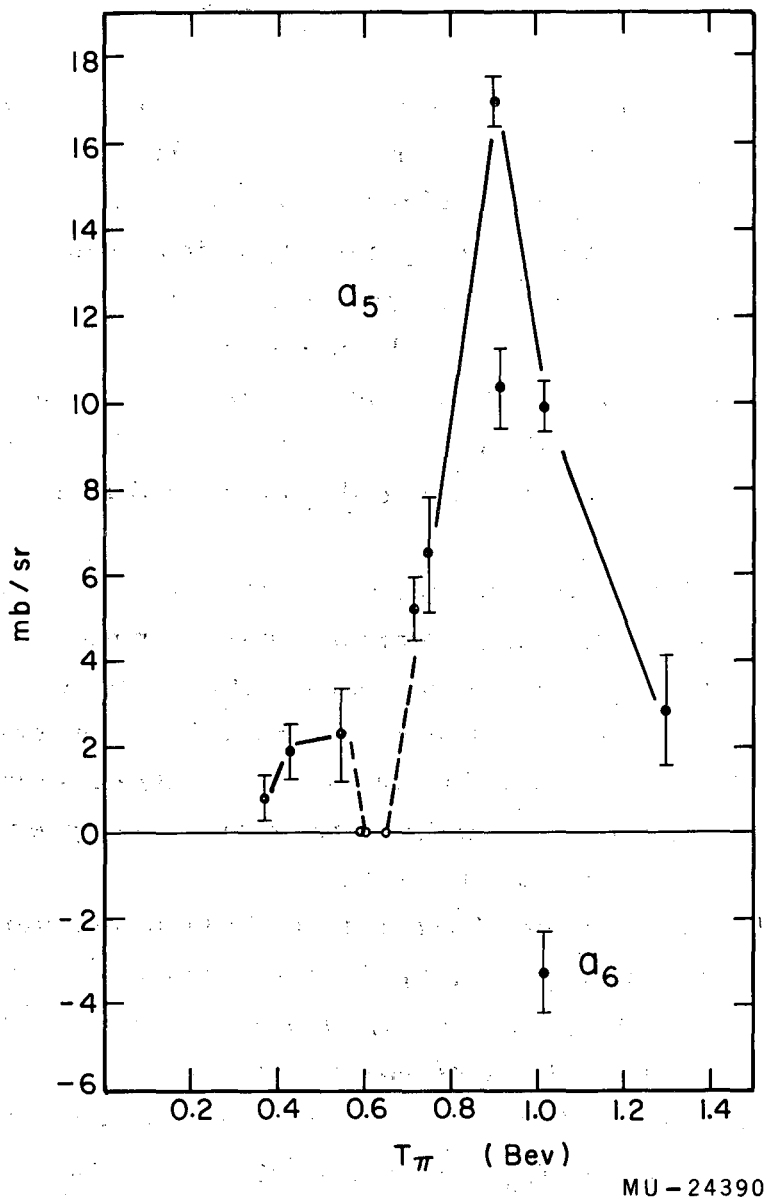

Fig. 31. Coefficients a_5 and a_6 in the cosine power series expansion of the angular distribution from $\pi^- + p \rightarrow \pi^- + p$ as a function of incident pion kinetic energy.

V. DISCUSSION

As an historical background to the discussion of my data, I present here a brief resumé of the thinking of some previous authors concerning the nature of the higher resonances.

Because the assignment of states appears to be less ambiguous for the photoproduction than for the scattering of pions at the higher energies, I consider it enlightening to review here the arguments of Peierls[55] that lead to an assignment of states on the basis of photoproduction data alone. His paper gives references to the development of photoproduction data and the theoretical thinking about the higher resonances.

By considering the transition matrix for the process written as a sum of contributions from all possible multipole transitions, Peierls predicts the angular dependence of the distribution of pions and the polarization of recoil protons for the first ten multipole transitions, and for certain combinations thereof. He then examines the data by making certain assumptions about the states present and then compares the data with the predictions.

He assumes first that, aside from the states known to be present from low-energy data, the higher resonance phenomena are due only to two new states, B and C, whose magnitudes $|M_B|$ and $|M_C|$ have maxima as functions of energy near the 750- and 1050-Mev peaks in the total cross section, respectively. The second assumption is that each of the peaks in σ_{tot} is due mainly to the single state to which it corresponds. He labels the 3, 3 resonant states A.

In identifying the states B and C, he determines five quantum numbers, defined as follows: J, the total angular momentum; ℓ, the orbital angular momentum; ω, the parity; T, the isotopic spin; and the sign of the amplitudes, $\lambda = M^+/|M^+|$.

If the states are assumed to be specific eigenstates of T and not mixtures, T is assigned a value of 1/2, because the contribution of these states B and C to π^+ production is much larger than the contribution to π^0 production.

He then assigns values for ℓ and J by examining the angular distribution data near each peak, where the corresponding state should predominate. For the production of π^0's near 750 Mev, the distribution is very like $(5 - 3x^2)$, which corresponds to a transition with $\ell = 1$ and $J = 3/2$, where $x = \cos\theta$. At 1000 Mev, he examines the π^+ distribution and concludes that $\ell = 2$ and $J = 5/2$ there.

Peierls' assignment of the parity quantum numbers is based partly on a study of the polarization of the recoil proton observed at 700 Mev (for $x = 0$), which implies a strong interference between states of opposite parity. If the interfering states in question are A and B, then $\omega_B = -1$. That C could be a main contributor to this interference is ruled out on several grounds. First, the lack of evidence for appreciable terms in x^4 in the angular distributions below 800 Mev implies that at 700 Mev $|M_C|^2$ is much smaller than $|M_A|^2 + |M_C|^2$. Second, the strange rise of a_2^+ for π^+ production near 500 Mev must be explained. The $a_2^{+,0}$ is a coefficient in the power series expansion of the angular distribution for $\pi^{+,0}$ production,

$$\frac{d\sigma}{d\Omega}^{+,0} = \sum_{k=0}^{n} a_k^{+,0} x^k, \qquad (21)$$

where $x = \cos\theta$. For $\omega_B = -1$, this comes from interference between B and the pure electric dipole, $J = 1/2$ production (S), and this interference is of the form $(3x^2 - 1)$. If this is the case, then $\lambda_B = +1$ is determined, also. On the other hand, for $\omega_B = +1$ and $\omega_C = -1$, then neither the interference of B with S (which is odd) or of C with S (which is isotropic) can explain this behavior. The interference of C with R (production from all possible transitions) can contribute to a_2^+, but this, together with the observed direction of the polarization, imposes requirements on λ_B and λ_C that would also imply a small a_1^+, which is not observed. Hence, we have $\omega_B = -1$. This assignment correctly predicts the sign of the polarization.

To determine ω_C and λ_C, Peierls observes that a_3^+ is already appreciable near 700 Mev and presumably is due to interference of C with the predominant terms at this energy. This can only happen for $\omega_C = +1$. The sign of a_3^+ gives the result $\lambda_C = +1$. The polarization has been measured in the region where interference between B and C might be expected, but it is small there because the ratio of $|M_c|$ to $|M_B|$ is small, and in fact the sign is uncertain. "It is interesting to note that only the large size of the 33 resonance compared with B, together with the change from a $T = 3/2$ to a $T = 1/2$ state, allows the energy at which $|M_A| = |M_B|$ to be close to the peak of B and the energy where $\delta_A - \delta_B = 90$ deg."

Table V summarizes Peierls' assignment of quantum numbers describing the second and third photoproduction resonances. The ℓ refers to the angular momentum of the initial state, $\gamma + p$.

Table V. Quantum numbers describing the second and third photoproduction resonances

Level	ℓ	J	ω	λ	T
A	0	3/2	+	-	3/2
B	1	3/2	-	+	1/2
C	2	5/2	+	+	1/2

After looking carefully at the picture presented by pion photoproduction, Peierls examines π-nucleon scattering and concludes, on the basis of the data then available, that scattering results cannot be entirely explained by the two $T = 1/2$ resonances. Nevertheless, he proposes a model for the existence of states B and C by assuming that the peak in the total cross section is due primarily to inelastic processes and only appears as a consequence in the elastic cross section. This

model and a similar model by Carruthers and Bethe[56] utilize the final-state 3, 3 isobar and π-π interactions to infer the importance of $D_{3/2}$ and $F_{5/2}$ states in the 600-Mev and 900-Mev resonances. These models also require absorption processes to be prominent.

Several other theoretical models have been proposed to explain the mechanism of the upper resonances. Wilson proposed a new isobaric state of the nucleon, similar to the $P_{3/2, 3/2}$ isobar,[18] but p-p scattering experiments gave no indication of isobars with masses corresponding to the $T = 1/2$ peaks, although they did show the 3, 3 isobar.[57] Wong and Ross conceived of successive rescattering of two pions with the nucleon and computed the recoupling amplitudes for rescatters.[58] Landovitz and Marshall proposed a model of pion-nucleon isobars, together with a π-π, $t = 1$ state interaction (excluding $t = 0, 2$), although they did not preclude other processes.[59] Carruthers saw the shoulder at about 850 Mev in the π^+-p cross section as being due to a $D_{3/2, 3/2}$ state that could influence the π^--p cross section, since the latter is a mixed state of $T = 1/2$ and $3/2$.[60] Peierls, commenting on the $D_{3/2}$ proposal of Carruthers, proposed a combination from the following final-state interactions: the second pion interacts in a $t = j = 1$ state with the first pion, and the second pion interacts with the nucleon in the 3-3 isobar.[42] He felt that a direct π-π (1, 1) interaction arising from one-pion exchange did not correlate with experiment. Pickup, Ayer, and Salant gave evidence of the π-π interaction;[61] Munir et al.[62] gave data that seemed to contradict the model of Carruthers and Bethe.[57] More recently, Carruthers has proposed a one-pion-exchange interaction like that of Peierls, together with a rescattering of one pion from the nucleon.[63] Most of these models also stress the importance of inelastic phenomena.

Data from previous scattering experiments have indicated several possibilities for the responsible quantum states. Erwin and Kopp[34] found that either P and D, or D and F waves fit the backward hump in their 950-Mev angular distribution. Walker, Hushfar, and Shepard[32] felt that a D state, coupled with a π-π interaction, was responsible for the enhancement of the total cross section near 900 Mev. Feld,

Maglić, and Diffey,[39] using emulsions, found better fits to their data with $D_{3/2} - F_{5/2}$ than with a $P_{3/2} - F_{5/2}$ assignment for the second and third peaks, respectively. Shonle[29] found either $P_{3/2} - D_{5/2}$ or $D_{3/2} - F_{5/2}$ to be consistent with his data. Brisson et al.[7] assigned $J = 5/2$ or $7/2$ to the third peak on the basis of the height of the "resonance" above a nonresonant background.

We now consider the data of this experiment. There are several interesting features to notice in the differential-scattering cross-section curves as we increase the incident pion kinetic energy (Figs. 23 through 27).

The backward hump in the distribution, which appears strikingly at 720 Mev, builds to an appreciable value at 900 Mev and dies down at 1020 Mev. This peaking of the hump is accompanied by a suppression of the cross section at 180 deg. Data on the angular distribution at 1.3 Bev[37] shows that the backward hump has essentially disappeared and that the value at 180 deg is definitely nonzero. This phenomenon of the backward hump arises from a contribution of the spin-flip scattering amplitudes (see Appendix A).

Data in the energy region below 550 Mev[26] do not show much forward peaking, whereas at 550 Mev we see the beginnings of very strong forward peaking, which is particularly evident at 900 Mev. The behavior of this peaking is indicated by the variation with energy of the dispersion relations point at 0 deg (see Table II). This strong forward peaking fits a diffraction model with an interaction volume of radius about 1.2 fermi, indicating that the incident pion interacts strongly with the meson cloud of the proton.

We notice that much of Peierls' argument[55] involves a study of the coefficients of the cosine power series expansion of the photopion angular distribution data. It is from such a study of the coefficients obtained from scattering data that we draw such conclusions as we feel are warranted by the data of this and previous experiments.

As seen from Figs. 29 through 31, the scattering at 600 Mev seems to be dominated by x and x^2 terms. If the scattering were due to a $D_{3/2}$ state without any $D_{5/2}$ present, we would expect no x^4 term; but we would expect the $D_{3/2}$ and $P_{3/2}$ amplitudes to interfere to

produce an x^3 term, which is thus conspicuous by its absence. However, if the D and P waves were to occur in the correct phase relationship, the x^3 term could disappear.

That a_3 builds up to a large value below 600 Mev indicates that there is a superposition of P and D waves below 600. The absence of a_4 indicates that the D-wave interaction is probably in a $J = 3/2$ state rather than $J = 5/2$.

A reasonable conclusion, then, is that $D_{3/2}$ amplitudes are present as we approach 600 Mev incident-pion kinetic energy and that the energy-dependent behavior of a_3 comes from the interference of the $P_{3/2}$ amplitude from the high-energy tail of the 200-Mev resonance, with the developing $D_{3/2}$ amplitude, and it is a fortuitous arrangement of the phase relation between the two that brings a_3 to zero near 600 Mev.

That a_4 and a_5 rise rapidly from 700 Mev to maxima at 900 Mev implies a strong superposition of F and D waves. The a_3 also has a negative maximum at 900 Mev, which may be due to the D-F interference and could indicate the presence of F- or P-wave interference with the D state. Since terms beyond x^5 are not required at 900 Mev, we infer that $F_{5/2}$ is probably the highest-order amplitude present there, although there is a possibility of some $F_{7/2}$ above 900 Mev, as indicated by the appearance of a small a_6 at 1020 Mev. Interestingly, there is no need of x^6 terms to fit the distribution obtained at 1300 Mev, although this may be due partly to the large errors associated with the data points at that energy.[37] At any rate the x^5 term does require D and F interference.

The backward hump in the angular distribution, which reaches a maximum near 900 Mev, together with the complete lack of scattering at 180 deg, requires a superposition of spin-flip amplitudes through F waves. The evidence seems to exclude an explanation of the 900-Mev resonance on the basis of a single ($F_{5/2}$) state in resonance, for at least D and F waves in strong superposition are required and, in view of the forward "diffraction" peaking of the angular distributions, absorptive processes may play a dominant role.

As Moyer[64] has mentioned, the D-F interference calls to mind the shoulder in the π^+-p total cross section, and the proposal of Carruthers[60] that it might be due to a $D_{3/2,\,3/2}$ state. Since π^--p scattering is a mixture of $T = 1/2$ and $3/2$ states in the proportion $1/3(T_{3/2}) + 2/3(T_{1/2})$, we might expect to see some manifestation of the $D_{3/2,\,3/2}$ state in π^--p scattering, although its effect is not seen in the π^--p total cross section in this energy region. If this 850-Mev phenomenon were indeed a D-state interaction, it would help to account for the strong D-F interference in the 720- to 1020-Mev region.

In summary, the data of this experiment are compatible with the models of Peierls[55] and Carruthers and Bethe,[56] which consider a π-N isobar and π-π interaction to infer the importance of $D_{3/2}$ and $F_{5/2}$ states at 600- and 900 Mev, respectively. The prominence of absorptive processes, as required in these models, is clearly indicated by the nature of the scattering angular distributions.

Hence, we are led to abandon the simple picture of single states in resonance, which was so successful around 200 Mev, as an explanation of the higher-energy phenomena.

ACKNOWLEDGMENTS

It is with great pleasure that the author acknowledges the benefit derived by him from the precept and example of Professor Burton J. Moyer, whose gentlemanly conduct and consummate skill as an educator combined to provide an experience highly profitable, in terms of human values as well as scientific understanding.

Thanks are due to Professor A. C. Helmholz for his guidance and help in the academic aspects of graduate study. Many valuable and original suggestions were made by Dr. Victor Perez-Mendez, whose experience helped the author avoid many of the pitfalls into which the inexperienced and often bewildered graduate student might stumble.

The author wishes also to thank Dr. Robert J. Cence for helpful advice during the analysis of the data.

Dr. Michael J. Longo contributed materially to the understanding and enlightenment of the author through his many suggestions and helpful criticism of the work.

A close bond of respect and friendship has been established through the close association of the author with Dr. Thomas J. Devlin. His never-failing willingness to contribute time and effort and well-considered suggestions added much to the success of the experiment.

Much helpful assistance was received in preparing and running the experiment from the following individuals: Mr. Dale Dickinson, Mr. Richard D. Eandi, Mr. Donald E. Hagge, and Mr. Paul J. McManigal. Also appreciated was the help given by Mr. Jagdish Baijal.

Of special mention is the invaluable assistance of Mr. Jerome A. Helland in writing the computer program that was used in reducing the data, as well as his great care in checking many of the author's calculations and in planning many aspects of the experiment.

Many other individuals contributed greatly to the experiment and the work of data reduction and presentation thereafter. The Bevatron staff and crew, under the direction of Dr. Edward J. Lofgren, provided the pion beam. Vital assistance in setting up the experimental equipment was provided by Wendell B. Olsen and his able crew. The

author is indebted to Mr. Howard E. Rogers for editing the manuscript and to Miss Miriam L. Machlis and Miss Carmen Aspuria for their careful typing.

The computer center of the Lawrence Radiation Laboratory provided an efficient method of data reduction.

The author feels a deep debt of gratitude to his loving wife, Dixie, who has borne and nurtured four beautiful children during his career both as an undergraduate and as a graduate student. Her patience during many lonely evenings and her bright spirit during times of frustration and discouragement gave great impetus to the labor and helped immeasurably in bringing this work to fruition.

This work was done under the auspices of the U. S. Atomic Energy Commission.

APPENDICES

A. Partial Waves

We give here a brief description of π^--p scattering in terms of phase shifts δ and scattering amplitudes f. The derivation of these formulae is straightforward and has been discussed, for example, by Bethe.[25] By way of notation, we write $\ell_\pm$ for the orbital angular momentum belonging to the total angular momentum states $J = \ell \pm 1/2$.

The non-spin-flip and the spin-flip amplitudes can be written as

$$f_a(\ell) = \frac{\lambda}{2i} \sum_{\ell=0}^{n} \left\{ (\ell + 1)(\eta_\ell^+ - 1) + \ell(\eta_\ell^- - 1) \right\} P_\ell^0(x), \tag{A-1}$$

and

$$f_\beta(\ell) = \frac{\lambda}{2i} \sum_{\ell=0}^{n} (\eta_\ell^+ - \eta_\ell^-) P_\ell^1(x), \tag{A-2}$$

respectively. In these two equations, $P_\ell^0(x)$ is the ℓth Legendre polynomial, and $P_\ell^1(x)$ is the associated Legendre function, both of which are functions of x, where $x = \cos\theta_3^*$, the cosine of the scattering angle in the center-of-mass system. The $\eta_\ell^\pm$ is associated with the phase shift $\delta_\ell^\pm$ by the relation

$$\eta_\ell^\pm = e^{2i\delta_\ell^\pm} . \tag{A-3}$$

In terms of these amplitudes, the differential cross section is written

$$\frac{d\sigma}{d\Omega^*} = |f_a|^2 + |f_\beta|^2. \tag{A-4}$$

In the energy region of this experiment, absorptive processes are important and can be described by introducing imaginary phase shifts, in analogy to the interaction of light in an absorptive medium.

Hence we write

$$\delta_\ell^\pm = a_\ell^\pm + i\beta_\ell^\pm , \tag{A-5}$$

which we combine with Eq. (A-3) to obtain

$$\eta_\ell^\pm = e^{-2\beta_\ell^\pm} e^{2ia_\ell^\pm}$$

$$= b_\ell^\pm e^{2ia_\ell^\pm} , \tag{A-6}$$

where $b_\ell^\pm$ is the absorption coefficient with the limits $0 \leqslant b_\ell^\pm \leqslant 1$. The $b_\ell^\pm = 1$ corresponds to no absorption of the ℓth wave. Thus we see that at higher energies we must consider not only higher ℓ values and the resulting increase in the number of parameters necessary to determine the problem, but also that the increased number of parameters is itself doubled if we want to consider absorption in a precise way.

The polarization P is written[65]

$$P \equiv (I_+ - I_-)/(I_+ + I_-), \tag{A-7}$$

where

$$I_\pm = |f_a \mp if\beta|^2$$

$$= (|f_a|^2 + |f_\beta|^2 \pm \mathrm{Im}\, f_a^* f_\beta). \tag{A-8}$$

Combining Eqs. (A-4), (A-7), and (A-8), we get

$$P = 2\,\mathrm{Im}\, f_a^* f_\beta \Big/ \left(\frac{d\sigma}{d\Omega^*}\right) . \tag{A-9}$$

From the definitions of f_a and f_β (Eqs. A-1 and A-2), and remembering that P_ℓ^1 is obtained by multiplying sin x times the first derivative of $P_\ell^0(x)$ with respect to x,

$$P_\ell^1(x) = \sin x \frac{d}{dx}\left[P_\ell^0(x)\right], \qquad \text{(A-10)}$$

we can readily see that a polarization experiment determines one less parameter for a given ℓ_{max} than does a differential-cross-section measurement. Also, because $P_\ell^1(x)$ contains the only sine terms in the expression for the angular distribution, any backward hump in that distribution must be due to the influence of f_β, the "spin-flip" term.

B. Criteria for Bevatron Targets

One would like to have a small Bevatron target, approaching a point source, for the beam optical system. At the same time, a counter experiment generally requires that the flux of secondary particles be maximized. In addition, one would generally like to minimize the production of electrons, although this may not always be important to a given experiment.

The relation between secondary particle flux and target size is given by

$$\frac{R}{R_0} = nx\sigma , \qquad \text{(B-1)}$$

where R_0 is the number of particles incident on the target, R is the number of particles interacting to produce the secondary beam, σ is the cross section per nucleon, x is the target length, and n is the effective number of nucleons per cc.

If we assume that σ is a constant, we must choose an x that is as large as possible consistent with the beam optical system, and we should maximize n if we are to maximize R.

We must first derive an expression for n. Let A be the total number of nucleons per atom, then

$$A = N + Z, \qquad \text{(B-2)}$$

where N is the number of neutrons, and Z the number of protons, per atom. A is then also defined as the number of grams per mole.

If we consider the "shadowing" effect of nucleons in a complex nucleus, the effective number of nucleons per atom is $A^{2/3}$. This classical approximation is pretty good for elements above beryllium (A = 9.013, Z = 4). The N_A is Avogadro's number, the number of atoms per mole, and ρ is the density in grams per cc. Then

$$n = A^{2/3} N_A \frac{\rho}{A} = N_A \frac{\rho}{A^{1/3}} . \qquad \text{(B-3)}$$

Figure 32 is a plot of n as a function of Z for most of the elements that might be used as Bevatron targets. Table VI lists these elements alphabetically, giving the chemical symbol, and Z, A, ρ,[66] and n for each listed element. In addition to pure elements, one might consider the use of alloys or compounds, such as alumina, as Bevatron targets.

To minimize electron production in the target, one should select his target from among the elements with relatively low Z. The target selected for use in this experiment was a 3-in. copper target.

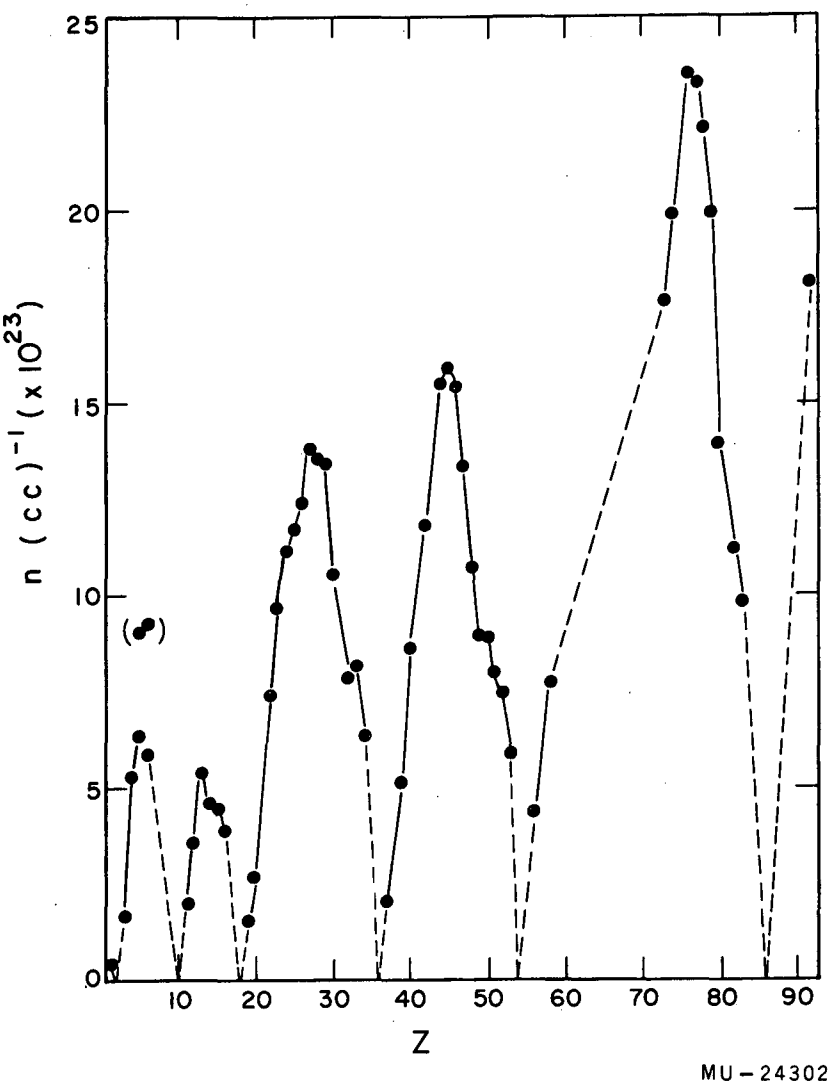

Fig. 32. Effective number of nucleons n as a function of Z.

Table VI. Table of elements that might be used as Bevatron targets, listing for each the chemical symbol, and Z, A, ρ in g/cc, and n, the effective number of nucleons per cc.

Element	Symbol	Z	A	ρ (g/cc)	$n(\times 10^{23})$ (cc^{-1})
Aluminum	Al	13	26.98	2.699	5.42
Antimony	Sb	51	121.76	6.618	8.04
Arsenic	As	33	74.91	5.73	8.19
Barium	Ba	56	137.36	3.78	4.41
Beryllium	Be	4	9.013	1.84	5.33
Bismuth	Bi	83	209.00	9.747	9.89
Boron (crystal)	B	5	10.82	3.33	9.07
Boron (amorphous)	B	5	10.82	2.34	6.37
Cadmium	Cd	48	112.41	8.648	10.79
Calcium	Ca	20	40.08	1.54	2.71
Carbon (crystal)	C	6	12.010	3.52	9.26
Carbon (graphite)	C	6	12.010	2.25	5.92
Cerium	Ce	58	140.13	6.79	7.87
Chromium	Cr	24	52.01	6.92	11.17
Cobalt	Co	27	58.94	8.9	13.77
Copper	Cu	29	63.54	8.9	13.43
Germanium	Ge	32	72.60	5.46	7.88
Gold	Au	79	197.2	19.3	19.97
Hydrogen(liquid)	H	1	1.0080	0.07095	0.426
Indium	In	49	114.76	7.28	9.02
Iridium	Ir	77	193.1	22.42	23.36
Iodine	I	53	126.91	4.94	5.92
Iron	Fe	26	55.85	7.87	12.40
Lead	Pb	82	207.21	11.005	11.20
Lithium	Li	3	6.940	0.534	1.69
Magnesium	Mg	12	24.32	1.741	3.62
Manganese	Mn	25	54.93	7.42	11.76

Table VI. (Continued)

Element	Symbol	Z	A	ρ (g/cc)	$n(\times 10^{23})$ (cc^{-1})
Mercury	Hg	80	200.61	13.546	13.94
Molybdenum	Mo	42	95.95	9.01	11.85
Nickel	Ni	28	58.69	8.75	13.56
Osmium	Os	76	190.2	22.5	23.56
Palladium	Pd	46	106.7	12.16	15.44
Phosphorus	P	15	30.975	2.34	4.49
Platinum	Pt	78	195.23	21.37	22.19
Potassium	K	19	39.100	0.87	1.54
Rhodium	Rh	45	102.91	12.44	15.99
Rubidium	Rb	37	85.48	1.532	2.10
Ruthenium	Ru	44	101.7	12.06	15.56
Selenium	Se	34	78.96	4.55	6.39
Silicon	Si	14	28.09	2.35	4.66
Silver	Ag	47	107.88	10.6	13.41
Sodium	Na	11	22.997	0.971	2.06
Sulfur	S	16	32.066	2.05	3.89
Tantalum	Ta	73	180.88	16.6	17.68
Tellurium	Te	52	127.61	6.25	7.48
Tin	Sn	50	118.70	7.29	8.93
Titanium	Ti	22	47.90	4.5	7.46
Tungsten	W	74	183.92	18.85	19.96
Uranium	U	92	238.07	18.7	18.17
Vanadium	V	23	50.95	5.96	9.68
Yttrium	Y	39	88.92	3.80	5.13
Zinc	Zn	30	65.38	7.10	10.61
Zirconium	Zr	40	91.22	6.44	8.62

C. Derivation of the Statistical Deviation

We derive here the probable deviation σ in the number of counts registered in the Cerenkov counter for a given number of monitor counts.[67]

The probability that C particles will radiate for M incident particles is simply

$$p^C q^{M-C}, \tag{C-1}$$

where p = the probability that a beam particle will emit Cerenkov radiation, q = the probability of no radiation, M = the number of counts in the pion beam monitor (i.e., the number of particles passing through the Cerenkov counter), C = the number of counts from the triple coincidence M + C (i.e., the number of particles that radiate), and $p = \lim_{M \to \infty} C/M$ (note: p + q = 1).

There are $\binom{M}{C}$ ways of selecting C particles from M particles, where $\binom{M}{C}$ are the binomial coefficients, so the probability becomes

$$w_M(C) = \binom{M}{C} p^C (1-p)^{M-C} \tag{C-2}$$

(note: $\sum_{C=0}^{M} w_M(C) = 1$).

Let us examine the identity

$$(py + q)^M = \sum_{C=0}^{M} \binom{M}{C} p^C y^C q^{M-C} = \sum_{C=0}^{M} w_M(C)\, y^C \tag{C-3}$$

Differentiate Eq. (C-3) once with respect to y to get

$$Mp(py+q)^{M-1} = \sum_{C=0}^{M} C w_M(C)\, y^{C-1}, \qquad (C-4)$$

and a second time with respect to y to get

$$M(M-1)p^2(py+q)^{M-2} = \sum_{C=0}^{M} C(C-1) w_M(C)\, y^{C-2}. \qquad (C-5)$$

We now let $y \to 1$ and see that

$$Mp = \overline{C}, \qquad (C-6)$$

and that

$$M(M-1)p^2 = \overline{C^2} - \overline{C}. \qquad (C-7)$$

If we combine Eqs. (C-6) and C-7), remembering that the dispersion $\sigma^2 = \overline{C^2} - \overline{C}^2$, we find that

$$\sigma^2 = Mp(1-p). \qquad (C-8)$$

Hence, the probable deviation in C is given by

$$\sigma = \sqrt{Mpq} \qquad (C-9)$$

$$= \sqrt{C(1-C/M)}. \qquad (C-10)$$

REFERENCES

1. R. Cool, O. Piccioni, and D. Clark, Phys. Rev. 103, 1082 (1956).
2. S. J. Lindenbaum and L. C. L. Yuan, Phys. Rev. 100, 306 (1955).
3. S. J. Lindenbaum and L. C. L. Yuan, Phys. Rev. 111, 1380 (1958).
4. H. C. Burrowes, D. O. Caldwell, D. H. Frisch, D. A. Hill, D. M. Ritson, R. A. Schluter, and M. A. Wahlig, Phys. Rev. Letters 2, 119 (1959).
5. J. C. Brisson, J. Detoeuf, P. Falk-Vairant, G. Valladas, L. Van Rossum, and L. C. L. Yuan, Phys. Rev. Letters 3, 561 (1959).
6. T. J. Devlin, B. C. Barish, W. N. Hess, V. Perez-Mendez, and J. Solomon, Phys. Rev. Letters 4, 242 (1960).
7. J. C. Brisson, J. F. Detoef, P. Falk-Vairant, L. Van Rossum, and G. Valladas, Nuovo cimento 19, 210 (1961).
8. Thomas J. Devlin, Jr., $\pi^{\pm}$-p Total Cross Sections in the Range 450 Mev to 1650 Mev (Ph. D. Thesis), Lawrence Radiation Laboratory Report UCRL-9548, March 6, 1961 (unpublished).
9. J. W. Dewire, H. E. Jackson, and R. M. Littauer, Phys. Rev. 110, 1208 (1958).
10. F. P. Dixon and R. L. Walker, Phys. Rev. Letters 1, 142 (1958).
11. F. P. Dixon and R. L. Walker, Phys. Rev. Letters 1, 458 (1958).
12. M. Feldman, V. Highland, J. W. Dewire, and R. M. Littauer, Phys. Rev. Letters 5, 435 (1960).
13. L. Hand and C. Schaerf, Phys. Rev. Letters 6, 229 (1961).
14. M. Heinberg, W. M. McClelland, F. Turkot, W. M. Woodward, R. R. Wilson, and D. M. Zipoy, Phys. Rev. 110, 1211 (1958).
15. J. M. Sellen, G. Cocconi, V. T. Cocconi, and E. L. Hart, Phys. Rev. 110, 779 (1958).
16. P. C. Stein and K. C. Rogers, Phys. Rev. 110, 1209 (1958).
17. J. I. Vette, Phys. Rev. 111, 622 (1958).
18. Robert R. Wilson, Phys. Rev. 110, 1212 (1958).
19. Freeman J. Dyson, Phys. Rev. 99, 1037 (1955).
20. Cf. e.g., Report of the Conference on Strong Interactions, Revs. Modern Phys. 33, No. 3 (1961).

21. Margaret H. Alston and Massimiliano Ferro-Luzzi, Revs. Modern Phys. 33, 416 (161).
22. Leroy T. Kerth, Revs. Modern Phys. 33, 389 (1961).
23. Such as, e.g., the principle of global symmetry.
24. Sergio Fubini, Revs. Modern Phys. 33, 455 (1961).
25. H. A. Bethe and F. de Hoffman, Mesons and Fields, Vol. 2: Mesons (Row, Peterson & Company, Evanston, Illinois, 1955), pp. 29-35, 63-70.
26. L. K. Goodwin, R. W. Kenney, and V. Perez-Mendez, Phys. Rev. Letters 3, 522 (1959).
27. R. R. Crittenden, J. H. Scandrett, W. D. Shephard, W. D. Walker, and J. Ballam, Phys. Rev. Letters 2, 121 (1959).
28. Gaillard et al., Compt. rend. 249, 1497 (1959).
29. John I. Shonle, Differential Elastic Pion-Proton Scattering at 600, 650, and 750 Mev (Ph.D. Thesis), Lawrence Radiation Laboratory Report UCRL-9362, Aug. 12, 1960 (unpublished).
30. J. Leitner, π^--p Scattering at 1.44 Bev (Ph.D. Thesis) Nevis Cyclotron Laboratories Report NEVIS 28, Jan. 1957 (unpublished).
31. Lee Baggett, Jr., π^--p Elastic Scattering and Single Pion Production at 0.939 Bev/c (M.S. Thesis), Lawrence Radiation Laboratory Report UCRL-8302, May 28, 1958.
32. W. D. Walker, F. Hushfar, and W. D. Shepard, Phys. Rev. 104, 526 (1956).
33. S. Bergia, L. Bertocchi, V. Borelli, G. Brautti, L. Chersovani, L. Lavatelli, A. Minguzzi-Ranzi, R. Tosi, P. Waloschek, and V. Zoboli, Nuovo cimento 15, 551 (1960).
34. A. R. Erwin, Jr., and J. K. Kopp, Phys. Rev. 109, 1364 (1958).
35. V. Alles-Borelli, S. Bergia, E. Perez Ferreira, and P. Waloscheck, Nuovo cimento 14, 211 (1959).
36. I. Derado, G. Lütjens, and N. Schmitz, Ann. Physik 7, 103 (1959).
37. M. Chrétien, J. Leitner, N. P. Samios, M. Schwartz, and J. Steinberger, Phys. Rev. 108, 383 (1957).
38. L. M. Eisberg, W. B. Fowler, R. M. Lea, W. D. Shephard, R. P. Shutt, A. M. Thorndike, and W. L. Whittemore, Phys. Rev. 97, 797 (1955).

39. B. T. Feld, B. C. Maglić, and C. A. Diffey, Bull. Am. Phys. Soc. II, 4, 447 (1959).
40. B. C. Maglić, B. T. Feld, and C. A. Diffey, Angular Distribution of Protons from π^--p Scattering at 900 Mev, Lawrence Radiation Laboratory Report UCRL-9594, Feb. 1961 (unpublished).
41. Ronald F. Peierls, Phys. Rev. Letters 1, 174 (1958).
42. Ronald F. Peierls, Phys. Rev. Letters 5, 166 (1960).
43. Jonathan D. Young, Optical Analog for a Symmetric Quadrupole, Lawrence Radiation Laboratory Report UCRL-9054, Jan. 22, 1960 (unpublished).
44. D. D. Newhart, V. Perez-Mendez, and W. L. Pope, Liquid Hydrogen Target, Lawrence Radiation Laboratory Report UCRL-8857, Aug. 18, 1959 (unpublished).
45. Lawrence Radiation Laboratory Counting Handbook, Lawrence Radiation Laboratory Report UCRL-3308 Rev., Jan. 1, 1959 (unpublished).
46. J. Atkinson and V. Perez-Mendez, Rev. Sci. Instr. 30, 864 (1959).
47. William A. Wenzel, Millimicrosecond Coincidence Circuit for High-Speed Counting, Lawrence Radiation Laboratory Report UCRL-8000, Oct. 2, 1957 (unpublished).
48. D. Swift and V. Perez-Mendez, Rev. Sci. Instr. 30, 1004 (1959).
49. Rossini and Deming, J. Wash. Acad. Sci. 29, 1121 (1957).
50. For a discussion of the normalization, not independently obtained in this experiment, see Sec. III-B-8 of this thesis.
51. D. Morgan, Some Theoretical Estimates of the Yield of Secondary Particles Produced by 7-Gev Protons, Atomic Energy Research Establishment (Harwell) Report AERE-R3242, 1960 (unpublished).
52. James W. Cronin, Phys. Rev. 118, 824 (1960).
53. Peter Cziffra and Michael J. Moravcsik, A Practical Guide to the Method of Least Squares, Lawrence Radiation Laboratory Report UCRL-8523 Rev., June 5, 1959 (unpublished).
54. Lester K. Goodwin, The Elastic Scattering of Negative Pions by Protons at 230, 290, 370, and 427 Mev (Ph. D. Thesis), Lawrence Radiation Laboratory Report UCRL-9119, April 7, 1960 (unpublished).
55. Ronald F. Peierls, Phys. Rev. 118, 325 (1960).

56. P. Carruthers and H. A. Bethe, Phys. Rev. Letters 4, 436 (1960).
57. G. B. Chadwick, G. B. Collins, C. E. Swartz, A. Roberts, S. de Benedetti, N. C. Hien, and P. J. Duke, Phys. Rev. Letters 4, 611 (1960).
58. Wen-Nong Wong and Marc Ross, Phys. Rev. Letters 3, 398 (1959).
59. L. F. Landovitz and L. Marshall, Phys. Rev. Letters 4, 474 (1960).
60. Peter Carruthers, Phys. Rev. Letters 4, 303 (1960).
61. E. Pickup, F. Ayer, and E. O. Salant, Phys. Rev. Letters 5, 161 (1960).
62. B. A. Munir, E. Pickup, D. K. Robinson, and E. O. Salant, Phys. Rev. Letters 6, 192 (1961).
63. Peter Carruthers, Phys. Rev. Letters 6, 567 (1961).
64. Burton J. Moyer, Revs. Modern Phys. 33, 367 (1961).
65. Michael J. Moravcsik, Phys. Rev. 118, 1615 (1960).
66. Handbook of Chemistry and Physics, ed. by Charles D. Hodgman (Chemical Rubber Publishing Co., Cleveland, Ohio, 1955) pp. 373, 1959.
67. Henry Margeneau and George M. Murphy, The Mathematics of Physics and Chemistry, 2nd ed. (D. Van Nostrand Company, Inc., Princeton, N. J., 1957) Sec. 12.4, pp. 438-442.